ANNUAL REVIEWS

Annual Review of Biochemistry

Imaging of DNA and RNA in Living Eukaryotic Cells to Reveal Spatiotemporal Dynamics of Gene Expression

Hanae Sato,[1,*] Sulagna Das,[1,*] Robert H. Singer,[1,2] and Maria Vera[1,3]

[1]Department of Anatomy and Structural Biology, Albert Einstein College of Medicine, Bronx, New York 10461, USA; email: hanae.sato@einsteinmed.org, sulagna.das@einsteinmed.org, robert.singer@einsteinmed.org

[2]Janelia Research Campus, Howard Hughes Medical Institute, Ashburn, Virginia 20147, USA

[3]Department of Biochemistry, McGill University, Montreal, Quebec H3G 1Y6, Canada; email: maria.veraugalde@mcgill.ca

Annu. Rev. Biochem. 2020. 89:159–87

First published as a Review in Advance on March 16, 2020

The *Annual Review of Biochemistry* is online at biochem.annualreviews.org

https://doi.org/10.1146/annurev-biochem-011520-104955

*These authors contributed equally to this article

Keywords

fluorescence microscopy, single-molecule techniques, nuclear organization, transcription, posttranscriptional regulation

Abstract

This review focuses on imaging DNA and single RNA molecules in living cells to define eukaryotic functional organization and dynamic processes. The latest advances in technologies to visualize individual DNA loci and RNAs in real time are discussed. Single-molecule fluorescence microscopy provides the spatial and temporal resolution to reveal mechanisms regulating fundamental cell functions. Novel insights into the regulation of nuclear architecture, transcription, posttranscriptional RNA processing, and RNA localization provided by multicolor fluorescence microscopy are reviewed. A perspective on the future use of live imaging technologies and overcoming their current limitations is provided.

Contents

1. INTRODUCTION

Eukaryotic cells are sophisticated multitasking units. They synthesize their components and control their quality, adapt to their microenvironment, and can divide to create new cells. These actions demand extraordinary coordination occurring in a small volume (average of 85 μm^3 in yeast and 5,700 μm^3 in neurons) packed with millions of molecules. Most knowledge about molecular interactions that lead to cell functionality originates from biochemical extraction of their components and assays performed in vitro to determine their functions. These approaches provide an overview of the cellular components in a population of cells but not their dynamics. To investigate when, where, and how components of a cell interact in situ, imaging these molecular events in living cells is necessary. In this article, the insights obtained from individual cells about the regulation of two critical biomolecules—DNA and RNA—are reviewed.

Recent advances in microscopy and fluorescent tagging technologies to label DNA loci and single RNA molecules in living cells have opened avenues to validate the results from biochemical approaches and gain novel insights into the behavior of molecules in their native environment. With the added dimension of time, precise kinetics of these molecular interactions can be quantified. The regulation of gene expression in different subcellular compartments, such as transcription in the nucleus (1–3), can now be visualized in real time in whole organisms (4, 5), and efforts are underway to study how nucleic acids mediate communication between the different compartments of the eukaryotic cell. Besides the well-defined compartments, the discovery of membraneless structures may facilitate molecular interactions in smaller microdomains in the nucleus and cytoplasm (6, 7). The fast dynamics of the assembly of these bimolecular condensates provide the means to regulate stochastic events, such as transcription in nuclear hubs (8, 9) or localization of RNAs in stress granules (SGs) upon stress (10–12). Therefore, visualizing molecules in living cells is a unique approach to study cell biology because it provides the means to integrate the cellular organization and the kinetics of basic physiological processes, such as DNA replication and RNA transcription and translation, in the life of a cell.

2. DETECTION OF DNA AND RNA FOR REAL-TIME IMAGING

The ability to visualize specific DNA loci and RNA molecules in living cells relies heavily on optical advances in fluorescence microscopy and engineering proteins or oligonucleotides that are

fluorescently tagged and bind the sequence of interest. Specific locus labeling allows one to characterize the locus behavior in its native genomic environment and functionally correlate it with its transcriptional status with temporal resolution. Additionally, the spatial context of the locus demonstrates how the dynamic formation of transcriptional hubs in certain nuclear territories regulates transcription. To this end, imaging of a single DNA locus should be accompanied by the visualization of the transcripts or the regulatory RNAs influencing the transcriptional outcome.

In this section, approaches to label DNA and RNA are summarized. The detection of these labeled molecules with precision relies heavily on the latest advances in fluorescence microscopy, which have been described in great detail in other reviews (13). Depending on the specimen being imaged (e.g., yeast, mammalian cells, or developing *Drosophila* embryos), the microscope and the illumination conditions need to be optimized. Different imaging modalities are available. Epifluorescence microscopes with scientific complementary metal–oxide–semiconductor and electron multiplying charge-coupled devices cameras work effectively for mammalian cells to capture fast temporal events, although out-of-plane light increases the background and may limit signal-to-noise ratios (SNRs). Strategies to limit out-of-plane fluorescence include total internal reflection fluorescence microscopy, highly inclined and laminated optical sheet illumination, and spinning disk confocal microscopy. These approaches have been widely used to image transcription factor (TF) dynamics; however, they have limited depth of illumination. To achieve high sample penetration depth, particularly for tissue or whole organisms, light-sheet fluorescence microscopy (LSFM) is the method of choice, in which a focused sheet of light is used to illuminate only a thin section of a sample (14). This structured light sheet increases acquisition speed and minimizes phototoxic damage to the cells, thereby enabling imaging of three-dimensional (3D) dynamics across large volumes (15). Therefore, by using a combination of microscopes and detectors, one can visualize both long-lasting events and processes that require fast image acquisition.

Detection of specific DNA loci or RNA with a high SNR is based on multimerizing fluorescent molecules. Alternative strategies to improve the SNR involve decreasing the fluorescence background by using fluorogenic aptamers and dyes, which are non-emitters in their unbound state and fluoresce only when bound to target nucleic acid sequences. As novel technologies for specific targeting emerge, combining new and existing approaches provides the means to interrogate DNA and RNA dynamics in living cells. Some of these approaches have provided single-molecule resolution (listed in **Table 1**), despite the challenges of nonrepetitive DNA sequences and individual RNA molecules.

2.1. DNA: Loci Tagging and Labeling

Chromatin architecture and dynamics have critical roles in the spatiotemporal regulation of gene expression in all eukaryotic cells. Although the spatial organization of a specific locus can be characterized using fluorescent in situ hybridization (FISH) on fixed cells, the dynamic interactions of chromatin during different stages of gene expression can only be addressed using live imaging methods. For a long time, these live imaging approaches mostly relied on the use of large arrays of the *lac* operator/Lac repressor (*lac*O/LacI) system, in which up to 256 *lac* operator (*lac*O) repeats were inserted into the genome. The fluorescently tagged *lac*O binding protein, Lac repressor, bound to these repeats with high affinity and specificity, providing the means to image chromatin dynamics in living cells and organisms (16–18). The analogous *tet* operator/Tet repressor (*tet*O/TetR) system employs a similar strategy (**Figure 1*a*, *i***). These arrays can be inserted into any DNA region of interest and are powerful approaches to image chromosome dynamics over long timescales, such as during cell division. With the advent of the clustered regularly interspaced short palindromic repeat–CRISPR-associated protein 9 (CRISPR-Cas9) system, these repeats could be targeted to specific genomic loci (19). Although these are robust approaches with

Table 1 Summary of molecules that have been labeled for live imaging, the labeling method used, and the biological process that was reported to be visualized

Category	Target	Single molecule detection	Biological phenomenon	Method(s) and Reference(s)
lncRNA	Xist	Yes	Chromatin dynamics	MS2-MCP (98), PUM-HD (99)
	TERRA	Yes	Chromatin dynamics	PUM-HD (71, 72), MS2-MCP (73, 74)
	NEAT1	Yes	Localization and foci detection	MB (157)
Small ncRNA	miRNA	Theoretically possible	Localization and foci detection	Activity-dependent modification (129)
	miRNA	No	Localization and foci detection	MB (158), Riboglow (55)
	Ribosomal RNA	No	Localization and foci detection	Aptamer (54)
	U6 RNA	No	Localization and foci detection	Aptamer (54)
	scaRNA	No	Localization and foci detection	Aptamer (54)
	mtRNA	No	Localization and foci detection	PUM-HD (159)
	snoRNA (snR30)	No	Localization and foci detection	Aptamer (160)
	U1 RNA	No	Localization in U bodies	Riboglow (55)
	U3 small nuclear RNA and 28S ribosomal RNA	No	Cellular and subcellular localization	ECHO-liveFISH in tissue (63)
mRNA	mRNA	Yes	Transcription, mRNA export, and localization	MS2-MCP (45), PUM-HD (64), MB (60), aptamer (115)
	mRNA	No	RCas9	RCas9 (65), Cas13a (66)
DNA	Xic	Yes	Chromatin dynamics	*tet*O/TetR system (95)
	Replication fork	Yes	Chromatin dynamics	TALE (67), *tet*O/TetR, and *lac*O/LacI systems (68, 69)
	Telomere	Yes	Chromatin dynamics	*lac*O/LacI system (70)
	Ribosomal DNA condensation	No	Chromatin dynamics	CRISPR (161)
	Chromosomal locus	Yes	Chromatin dynamics	dCas9-SunTag system (160a), CRISPR liveFISH (33)
	Loci interactions	Yes (single locus detection)	Chromatin compaction, decompaction, and interaction	*tet*O/TetR and *lac*O/LacI systems (4, 91), CRISPR (20), and CRISPRainbow (29)

Abbreviations: Cas, CRISPR-associated; CRISPR, clustered regularly interspaced short palindromic repeat; dCas9, catalytically inactive Cas9; ECHO-liveFISH, exciton-controlled hybridization-sensitive fluorescent oligonucleotide live fluorescent in situ hybridization; *lac*O/LacI, *lac* operator/Lac repressor; lncRNA, long noncoding RNA; MB, molecular beacon; MCP, MS2 capsid protein; miRNA, microRNA; mtRNA, mitochondrial RNA; ncRNA, noncoding RNA; NEAT1, nuclear enriched abundant transcript 1; PUM-HD, pumilio homology domain; RCas9, RNA-targeting Cas9; scaRNA, small Cajal body–specific RNA; snoRNA, small nucleolar RNA; TALE, transcription activator-like effector; TERRA, telomeric repeat-containing RNA; *tet*O/TetR, *tet* operator/Tet repressor; Xic, X-inactivation center; Xist, X-inactive specific transcript.

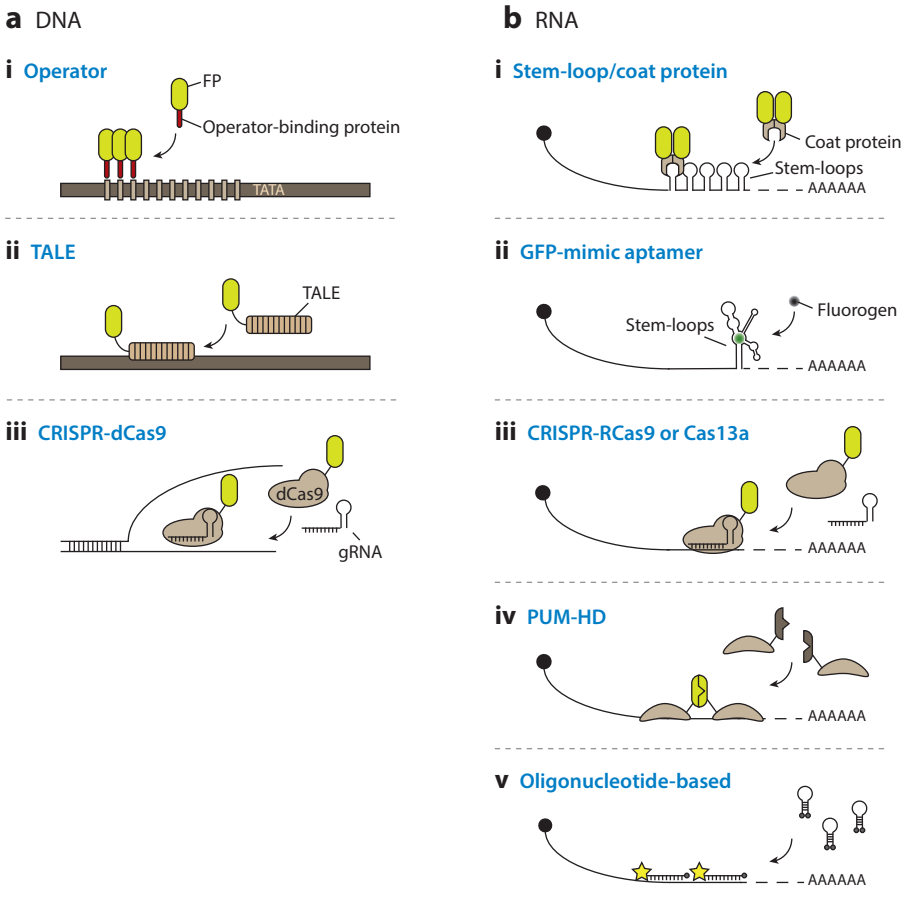

Figure 1

Fluorescent imaging approaches for DNA/RNA detection in living cells. (*a*) Detection of genomic DNA at single-locus resolution in living cells. (*i*) Fluorescent protein (FP)-labeled operator-binding proteins are tethered to multiple repeats of an operator inserted into a desired DNA locus (e.g., *lac* operator/Lac repressor and *tet* operator/Tet repressor systems). (*ii*) Transcription activator-like effectors (TALEs): TALEs are DNA-binding proteins that can be designed to target any DNA sequence (21). Customized FP-tagged TALEs can be tethered to specific endogenous genomic loci and imaged. (*iii*) Clustered regularly interspaced short palindromic repeat (CRISPR)-catalytically inactive Cas9 (dCas9): FP-tagged dCas9 is tethered to specific endogenous genomic loci that are recognized with specific guide RNA (gRNA). (*b*) Single-molecule RNA detection in living cells. (*i*) The stem-loop/coat protein system is composed of a specific RNA stem-loop structure inserted into desired mRNAs [e.g., MS2–MS2 coat protein (MCP), PP7–PP7 coat protein (PCP), λN-boxB] and an FP-labeled RNA-binding protein (coat protein) binding to the stem-loops with high affinity and specificity. (*ii*) Green fluorescent protein (GFP)-mimic aptamer: RNA aptamers inserted into desired mRNAs are labeled with fluorogenic ligands (fluorogens) that specifically recognize the aptamer (e.g., Spinach, Mango). (*iii*) CRISPR-RCas9 or Cas13a: This approach is based on CRISPR-dCas9 for DNA labeling, but RNA-targeting Cas9 (RCas9) or Cas13a is used for the specific labeling of desired endogenous mRNAs. (*iv*) Pumilio homology domain (PUM-HD): PUM-HD is an RNA-binding protein domain that can be designed to bind any eight-base RNA sequence. A pair of adjacent endogenous RNA sequences is labeled with biomolecular fluorescence complementation using designed PUM-HD tagged with FP fragments. (*v*) Oligonucleotide-based: Also known as fluorescence in vivo hybridization, complementary oligonucleotides with synthetic fluorescence dyes target desired mRNAs with RNA–DNA base paring (e.g., molecular beacons, forced intercalation probes, and quenched autoligation probes) (62).

high SNRs, the insertion of these long arrays could affect chromatin structure and the function of the targeted loci (20). This problem was circumvented by programming DNA-binding proteins, such as zinc fingers or transcription activator-like effectors (TALEs), to bind to specific DNA sequences. These proteins are fused to a fluorescent protein or quantum dots and work effectively for labeling repetitive DNA (21–23) (**Figure 1*a*, *ii***). However, their low SNR and inefficient multimerization limit their use for labeling DNA. In recent years, the CRISPR-Cas9 system has proved effective at directing the targeting and labeling of specific chromosomal loci with high precision. The first study used an enhanced green fluorescent protein (EGFP)-tagged catalytically inactive Cas9 (dCas9) protein and a structurally optimized small guide RNA (sgRNA) to image repetitive elements in telomeres and coding genes (24) (**Figure 1*a*, *iii***). While this method allowed for visualization of telomere dynamics and Mucin 4 [a highly repetitive sequence (25)], its ability to label nonrepetitive genomic sequences was not robust. The dCas9 system led to a gamut of labeling strategies for imaging any loci of choice in various cell types (26).

The combination of CRISPR-Cas9 with the bacteriophage-derived RNA stem-loop motifs MS2 and PP7 (see Section 2.2) made it possible to simultaneously visualize two distinct genomic loci. The design involved sgRNAs containing MS2 and PP7 aptamers that are bound by fluorescently tagged MS2 capsid protein (MCP) and PP7 coat protein (PCP), respectively (20, 27). This technology labels an individual chromosomal locus with as few as four unique sgRNAs and renders nonrepetitive regions of the genome visible for live imaging. For a more flexible labeling of multiple genomic loci in living cells, two adaptations of the CRISPR-Cas9 system have been made: (*a*) multicolor versions of CRISPR specifically using dCas9 from three bacterial orthologues (28) and (*b*) engineered sgRNAs that can bind to combinations of different fluorescent proteins, also known as the CRISPRainbow system (29) (**Table 1**). CRISPRainbow utilizes sgRNAs that have been genetically modified at their 3′ end to be tagged with a pair of any of the three RNA aptamers (MS2, PP7, and λN-boxB). The cognate coat proteins are fused to spectrally distinct fluorescent proteins, allowing each sgRNA to be bound by a pair of the same or different coat proteins. Depending on the stem-loop pair on the RNA, up to six combinations of colors can be generated using primary fluorophores (red, green, and blue) when sgRNAs have identical aptamer pairs, or three secondary colors can be generated using pairs of different aptamer sequences that bind to two distinct proteins. This multiplexing approach enables the simultaneous imaging of up to six chromosomal loci in living cells and reveals their dynamic interactions. While CRISPRainbow represents a significant technological advancement for genomic DNA imaging, the unbound sgRNAs that contribute to the background, as well as the variable quantum yield of different fluorescent proteins, may limit its utility for long-term imaging with high sensitivity in living cells. An improved multicolor CRISPR-based imaging system increases the stability of the guide RNAs (gRNAs) by inserting octet arrays of stem-loop aptamers at the 3′ end of the gRNA scaffold. This CRISPR-Sirius system confers multiple loci tracking with increased brightness, a big technological leap for imaging low-copy genomic loci or single-copy genes (30).

Approaches employing dCas9 and an engineered sgRNA harboring a unique molecular beacon (MB) target sequence (sgRNA-MTS) may provide more flexibility and lower background (31). MB is an RNA labeling method using single-stranded oligonucleotide probes with a fluorophore and a quencher at the two ends (see Section 2.2). In contrast to the sgRNA-MTS approach, which detects highly repetitive elements, the most recent version of the CRISPR-MB system, CRISPR–dual-fluorescence resonance energy transfer (FRET) MB, enables imaging of nonrepetitive loci with higher specificity (32). The binding of two distinct MBs with a FRET fluorophore pair to the same gRNA causes the FRET emission. Only when two MBs bind to a gRNA that targets the specific genomic locus does this approach achieve imaging of nonrepetitive genomic loci with higher specificity. The CRISPR-MB system may provide flexibility in choosing any

combination of target sequence and MBs; however, the efficacy of hybridization and stability of the MBs need to be characterized in detail.

Instead of expressing CRISPR components in living cells, dCas9-EGFP and Cy3-labeled gRNA can be assembled in vitro to form complexes called fluorescent ribonucleoproteins (fRNPs) that are delivered into cells using electroporation (33). A higher SNR was achieved by stabilizing DNA-bound fRNAs, while most unbound gRNAs were degraded within 4 h. This CRISPR LiveFISH method was applied to label DNA and RNA using dCas9 and dCas13, respectively, enabling simultaneous visualization of genomic DNA and RNA transcripts in living cells. The dual DNA-RNA LiveFISH approach, combined with other genetic manipulation technologies, will prove to be a powerful tool to interrogate the causal relationships between genome organization and transcription dynamics.

2.2. RNA: mRNA and Noncoding RNAs

mRNA was the first molecule to be viewed at single-molecule resolution in living cells through the use of a strategy to introduce a tandem array of bacteriophage-derived stem-loops (referred to as MS2) into the endogenous locus of a gene (34). MS2 is an RNA aptamer that can be multimerized and integrated within the intron, coding sequence, or untranslated region (UTR) of a transcript as an array. Most studies utilize arrays of 24 stem-loops at the 3′ UTR; however, array lengths may vary from 12 to 128 repeats, depending on the gene of interest, sensitivity of detection, and timescales of imaging. Each stem-loop is tightly bound by the coat protein (MCP) and fused to fluorescent proteins. MS2–MCP–fluorescent protein binding renders a single mRNA visible because it is decorated with multiple fluorescent molecules (**Figure 1*b, i***). Several versions of the MCP–fluorescent protein have been used, with the best so far being a tandem MCP fused to two fluorescent proteins for bright and homogenous labeling of mRNAs (35). Tagging methods analogous to the MS2-MCP system, such as PP7, U1, and λN-boxB, have been developed over the years, conferring the ability for multiplexed mRNA imaging in living cells (36–38). Owing to the central role of mRNA in gene expression, quantification of the imaging data has provided unprecedented insights into the regulation of transcription, mRNA export and localization, and, more recently, translation and decay (1, 2, 36, 38–43). The MS2 and PP7 systems have been reengineered over the years to accommodate the demands of specific biological questions (44, 45). One such example is the latest MS2 version with reduced affinity for the MCP to overcome the challenges of degradation of the MS2-MCP cassette, as observed in yeast (45–48). Although this tagging technology requires introducing MS2 aptamer repeats into RNAs, these reporter systems have faithfully captured the fate of single mRNAs without significantly perturbing their endogenous regulation. In fact, several mouse models of genes tagged with either the MS2 or PP7 technology are available that do not show any effect on gene function; these can now be used to monitor the behavior of mRNAs in living tissue (49–51). Nonetheless, genetic modifications must insert the cassette into the genome to tag the transcribed mRNA and must express the fluorescent binding protein. These requirements preclude the tagging of small noncoding RNAs (ncRNAs) that will experience an unnatural increase in size by more than a kilobase that will probably interfere with their proper folding, processing, and biological function.

An alternative strategy to eliminate the protein component of the MS2-MCP and its equivalent systems was to make an RNA aptamer that could fluoresce on its own. Spinach and Broccoli aptamers were the first iterations (52, 53), but these RNA mimics of GFP have poor folding properties in vivo, low quantum yields, and rapid photobleaching. Two recent approaches that partially overcame these caveats are the Mango III fluorogenic aptamer and the Riboglow modular system (**Figure 1*b, ii***). Mango III is a closed RNA stem with a space to bind with high affinity to thiazole

orange 1 dye–biotin and increase its quantum yield to 1,000 times the initial yield when it binds with its ligand. It is more photostable than the aptamer Broccoli and has been successfully used to localize RNA polymerase III (RNAP III)-dependent transcripts such as 5S and U6 RNAs (54). The Riboglow system is based on the bacterial cobalamin riboswitch RNA. Cobalamin quenches the fluorescence of a synthetic fluorophore until it is bound to the RNA riboswitch (55). The increase in the quantum yield of the fluorophore probes and their stability enables it to localize U1 small nuclear RNP in Cajal bodies in the nucleus and U1 bodies in the cytoplasm. Thus, Riboglow provides an alternative system to visualize only highly expressed ncRNAs in live mammalian cells. Two new fluorogenic aptamers, both called Peppers, have been recently developed to either increase the spectral range of RNA labeling (56) or introduce a fluorogenic protein component that is stabilized by RNA binding (57). In general, fluorogenic aptamers are not as bright as fluorescent coat proteins, and, as with the MS2 system, they demand genetic insertion to tag the RNA under investigation.

Several systems attempt to circumvent the problem of genetic insertion to tag endogenous RNAs. Examples are oligonucleotide-based RNA detection (also known as fluorescence in vivo hybridization), pumilio homology domain (PUM-HD), and the RNA-targeting Cas9 (RCas9) or Cas13a system (**Figure 1*b*, *iii–v***; **Table 1**). One oligonucleotide-based approach is the MB, which contains a fluorophore or a quencher at each end of the oligonucleotide (58). In the absence of its target sequence, MBs have very low background fluorescence due to the formation of a stable duplex system whereby the quencher significantly quenches the fluorophore. Upon hybridization of the MB to a complementary sequence, the duplex is disrupted, leading to fluorescence emission. The latest version is the ratiometric bimolecular beacons (RBMBs), which are two-component MBs (59). The first component is a stem-loop-forming oligonucleotide with one fluorophore that is quenched by the second component, an antisense oligonucleotide of the stem tagged at both ends. The end closest to the stem-loop has the quencher, and the distal one has a spectrally different fluorophore. Binding of the RBMB to the target mRNA switches the labeling of the RBMB from one to two fluorophores. This ratiometric approach decreases the false positive signals obtained from mislocalization of MBs in the nucleus (60). RBMBs have been successfully used to track the motion of single RNAs in living cells (61). Several other oligonucleotide-base approaches have been attempted, such as forced intercalation probes and quenched autoligation probes (62). A recent example is the visualization of the 28S ribosomal RNA and U3 snRNA intranuclear foci dynamics in the brain after in vivo electroporation of exciton-controlled hybridization-sensitive fluorescent oligonucleotide (ECHO)-liveFISH probes (63). General limitations of oligonucleotide-based RNA detection approaches are the low SNR, the requirement for injection of fluorescence-labeled oligonucleotide, the trapping of probes by endosomes, and the low target specificity.

An alternative approach for labeling an endogenous RNA sequence is the PUM-HD system, a programmable RNA-binding protein that targets any eight-base RNA sequence (64). Since it recognizes a short RNA sequence, the specificity of labeling and the possibility of off-target effects limit this approach. Specificity has been achieved with the catalytically inactive Cas13a system and RCas9 by using a mismatch protospacer-adjacent motif (PAM) as part of the oligonucleotide that binds the RNA sequence. These systems do not elicit the activity of RNAseH and report on mRNA localization through a fluorescently tagged Cas9 (65, 66). The caveat of the MB, PUM-HD, and RCas9 systems is that they cannot achieve single-molecule resolution unless several of these molecules are delivered to the cell and bind to specific sequences of the same mRNA. Hence, although promising for RNA tagging, much work needs to be done to improve their brightness and make small RNAs visible.

Overall, there is a plethora of systems engineered to visualize RNAs during their life cycle, and their use depends on the experimental requirements that will answer a specific biological question. As of today, the most used RNA tagging systems are the MS2 and analogs because they provide long-term single-molecule tracking. This review provides several examples of live imaging technologies used to investigate posttranscriptional RNA processing, localization, and fate and to address fundamental cellular processes such as chromatin remodeling, nuclear organization, and transcription (**Figure 2**).

3. DNA REPLICATION AND TELOMERE DYNAMICS

DNA replication is a fundamental process in proliferating cells. The precise duplication of DNA prior to mitosis is tightly controlled during development and cell differentiation. In *Drosophila*, embryonic developmental progression extends the duration of the cell cycle. Using the TALE system to tag two specific DNA satellite sequences, one in the X chromosome and another in each of the two autosomes, researchers showed that developmental progression altered the timing of the replication of those two satellites independently (67). Live DNA imaging shed light on the heterogeneity of the replication rates as fly development progressed: Although both satellite sequences showed an overall delayed timing of initiation and increased duration of replication with mitotic cycles, the replication rates of the two satellite sequences varied depending on the cycle number. During mitotic cell division, a precise program controls the initiation timing of different origins of replication. In single DT40 chicken cells, the activity of six single loci was monitored using the *tet*O/TetR system (68). The quantitative detection of the allelic asynchrony at these loci revealed the stochasticity of the programed replication initiation timing. In addition, the correlation between nuclear positioning and the allelic synchrony in late replicating loci suggested the strict control of replication timing close to nuclear lamina.

The replication rates of single replicating forks were measured in yeast using the labeling of two adjacent DNA loci with the *lac*O/GFP-LacI and *tet*O/tdTomato-TetR systems (69). The study found the impact of major leading and lagging replication factors on the replication rates of single replicating forks. Fast temporal imaging of these loci showed that the replication of a 30-kb sequence took 12–15 min, as calculated from the difference in the duplication time between the fluorescent signals. Unexpectedly, the polymerase accessory subunits made a limited contribution in determining replication rates, but maturation of the Okazaki fragment was crucial for the fork progression (69).

Each cell division is accompanied by the shortening of the telomeres. Telomeres are unique structures that cap the end of chromosomes and protect their ends from sticking to each other. The telomere length depends on the addition of the telomere repeat sequence by the RNP telomerase. Telomerase has an ncRNA [telomerase component 1 (TLC1)] that is used as a template with binding proteins that catalyze the addition of the repeat sequence to the 3′ end of telomeres. The telomerase recruitment to the telomeres during the cell cycle was tracked by tagging TLC1 with the MS2-MCP system (70). Single-molecule tracking of TLC1 molecules showed that they freely diffuse during the G_1 and G_2 phases of the cell cycle but colocalize with telomere loci, labeled with the *lac*O/LacI system, in late S phase. Telomerase associates longer (up to 45 s) at the telomere in S phase than in G_1 phase (5 s). The telomere sequence, a six-nucleotide repeat, is also transcribed into a functional long ncRNA (lncRNA), the telomeric repeat-containing RNA (TERRA). TERRA participates in telomere biogenesis, inducing its heterochromatin formation and capping of the telomere. Imaging approaches have addressed TERRA localization and molecular dynamics in human cells (71, 72) and yeast (73, 74). Single TERRA molecules were visualized with either the MS2-MCP system or the PUM-HD system

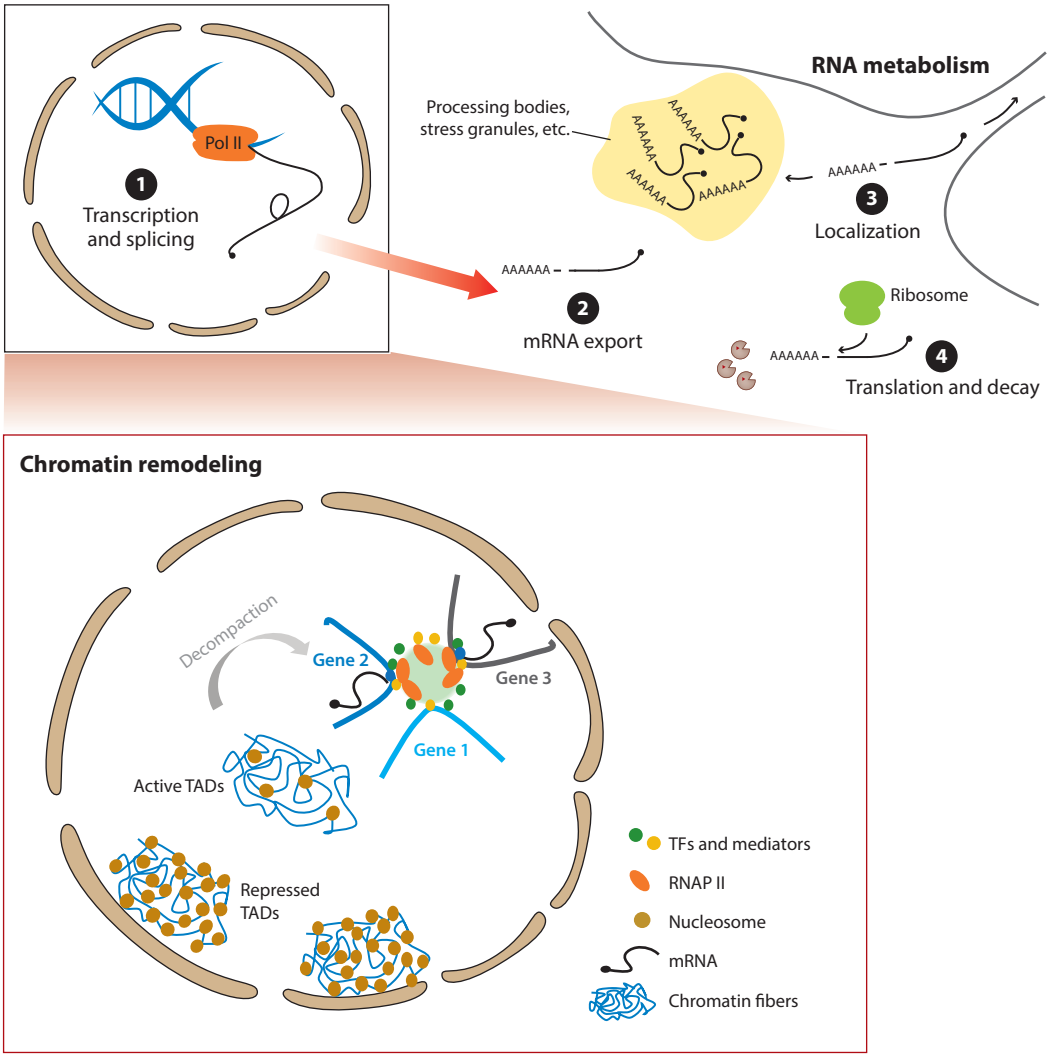

Figure 2

Cellular processes addressed using single-molecule imaging approaches. Single-molecule imaging approaches have been applied to visualize the processes occurring in the nucleus and cytoplasm: remodeling of chromatin and RNA metabolism. The illustration summarizes the cellular processes characterizing the molecular dynamics, kinetics, and temporal order of events using live imaging approaches. The overall life cycle of the mRNA from step ❶, transcription, to step ❹, decay, in the different subcellular compartments is shown. Translation may occur before or after step ❸, mRNA localization, depending on the mRNA and the cell response to environmental clues. The inset for chromatin remodeling shows a magnified view of the nucleus, where DNA associated with histones (nucleosomes) is organized into topologically associated domains (TADs). These sequences within TADs self-interact with each other more frequently than do sequences outside TADs. TADs may be repressed, often when they are associated with the nuclear lamina, or they may become more flexible domains regulating transcription (active TADs). Following decompaction of the chromatin, active transcription from multiple genes may occur simultaneously (e.g., Genes 2 and 3) when they share the same transcriptional hub. The shaded green area indicates a protein-rich core, housing transcription factors (TFs), mediators, and RNA polymerase II (RNAP II).

against the repetitive UUAGGG sequence. TERRA is transcribed from short telomeres (73). It freely diffuses, forms foci, and transiently colocalizes with the heterogeneous nuclear ribonucleoprotein hnRNPA1 (71) and the telomere (72, 73). Although these reports identified TERRA foci and their colocalization with some regulatory factors, additional approaches are needed to understand the diverse functions of TERRA on telomere biogenesis.

DNA replication and the complex dynamics of factors affecting chromosome integrity advocate for a regulatory role of nuclear organization as well as the roles of specific proteins and ncRNAs.

4. SPATIOTEMPORAL DYNAMICS OF GENE EXPRESSION IN THE NUCLEUS

4.1. Chromatin Architecture Regulates Gene Expression

In the nucleus, the genome is highly organized and compacted into the 3D volume to form higher-order chromatin structures (75, 76). The configuration of the chromatin is regulated in a dynamic manner and determines the spatial and temporal features of replication, transcription, and gene silencing. In this section, we review the different examples of how chromatin organization affects loci interactions and gene activation.

4.1.1. Higher-order chromatin structure and heterochromatin organization. Chromatin organization occurs at multiple levels, from nucleosomes (DNA wrapped around histones) to epigenetic modifications of histones, higher-order domains such as heterochromatin and euchromatin, and finally the physical movement of chromatin and long-range interactions. Technologies such as chromosome conformation capture (3C and Hi-C) have yielded high-resolution contact probability maps of the genome (77). This has led to the identification of self-interacting genomic regions known as topologically associated domains (TADs) in various cell types (78). TADs play instructive roles in transcriptional regulation, and direct visualization of TAD organization at gene clusters (such as the *HoxD* locus in embryonic stem cells) has been done in fixed cells (79, 80). How these TADs are formed and maintained by a functional interplay of cohesins and CCCTC-binding factors (CTCFs) is only beginning to be visualized in real time by imaging of the factors (81). Recent work has highlighted how these CTCFs self-organize and form chromatin loops in a locus-specific mechanism, a process potentially regulated by RNA or RNAs (82).

Progress has also been made in imaging single nucleosomes by single-molecule tracking photoactivated localization microscopy, exhibiting that they form compact domains, frequently in the heterochromatin region (83). These transcriptionally repressed heterochromatin domains are epigenetically defined by the methylation of histone H3 at lysine 9 and recruitment of its binding partner HP1α. Real-time imaging of HP1α in cells, along with a transgene array labeled with both the *lac*O and MS2 systems, allowed researchers to monitor the dynamics of HP1α association with chromatin and its impact on transcription (84). The study characterized how the dynamic loss of HP1α from the heterochromatin and an exchange of histones mediates transition into a transcriptionally active state. More studies on the dynamic behavior of HP1α protein have revealed that the protein can undergo liquid-liquid demixing in vitro and phase separate to form heterochromatin domains (85). The domain formation is sensitive to disruption of weak hydrophobic interactions and exhibits restricted diffusion of molecules. These features are conserved across different isoforms of human HP1 and dependent on the phosphorylation status of the protein (86). It remains to be elucidated how the nuclear environment promotes such domain formation or whether it is an intrinsic property of these proteins. In the future, imaging technologies to correlate HP1α clustering dynamics with the genomic loci interactions will be important to resolve how higher-order nuclear organization is achieved and its effect on transcription.

4.1.2. Chromosome, decompaction, interactions, and gene expression. The physical interactions between DNA regions, particularly between enhancers and promoters, are known to impact gene expression, as shown by 3C and Hi-C studies (77, 87). These interactions can occur both in *cis* and in *trans*. *Trans* interactions, in which the enhancer of one chromosome interacts with the promoter of another chromosome, are an example of long-distance interactions in the nucleus. Recent work has shown that insulators play an instructive role in aligning the two alleles and facilitate this transcoactivation. This phenomenon, known as transvection, has been imaged in *Drosophila* by inserting MS2 and PP7 stem-loops into reporter mRNAs transcribed from homologous alleles on complementary chromosomes (88, 89). One of the alleles has the enhancer, which is shared, resulting in coactivation of PP7 and MS2 reporter genes both in *cis* and in *trans*. This sharing of resources during coactivation of genes aligns with the emerging concepts of formation of transcriptional hubs with observed clustering of RNAP II and associated activators.

To understand the causal relationship between macroscale 3D organization and gene expression, a programmable 3D genome organizer named CRISPR-GO has been designed by coupling the CRISPR-dCas9 system with nuclear compartment–specific proteins (90). This allowed an inducible system for dynamic repositioning of specific genomic loci to different nuclear compartments, such as the nuclear periphery, Cajal bodies, and promyelocytic leukemia bodies. By combining CRISPR-GO with live-cell CRISPR-Cas9 imaging, the real-time interactions of chromatin with the nuclear compartments were elucidated: For example, targeting loci to Cajal bodies repressed gene expression of not only the reporters but also the distal endogenous genes. This study shed light on how genome positioning and the environment may be instrumental in determining transcription from these loci. While the macroscopic interactions could be mapped out, the higher-order interactions enabling transcription from one compartment versus another remain to be characterized.

Dynamic changes in chromatin architecture and chromosomal localization are related to the transcriptional status of genes. To quantify the changes in chromatin conformation in response to transcriptional activation, compaction of the *GAL* locus was visualized in single live *Saccharomyces cerevisiae* (91). The *GAL* locus extends for 31 kb in the DNA and contains the *GAL7*, *GAL10*, and *GAL1* genes, which are transcriptionally active when the carbon source in growth media is changed to galactose. The impact of transcription on chromatin decompaction was measured by inserting an array of *lac*O loops labeled with GFP and an array of *tet*O sequences labeled with mCherry in two different positions on the *GAL* locus. The intermolecular distance between the two fluorescent foci doubled during transcriptional activation compared to inactivate states, suggesting ongoing chromatin decompaction during this process. This decompaction was triggered by nucleosome eviction by the SWItch/sucrose nonfermentable (SWI/SNF) nucleosome remodeler complex and by transcription initiation. Although the direct role of transcription progression on chromatin structure remains to be deciphered, this result indicates the absence of promoter–terminator looping in the *GAL* locus. Unexpectedly, histone acetylation affected neither transcription nor the level of chromatin compaction. These findings differ from those of a previous study showing that the acetylation of histone H3 at lysine 27 (H3K27ac) primes a robust transcriptional response of the glucocorticoid receptor (GR) in mammalian cells upon hormone stimulation (92). The dynamics of histone modifications and RNAP II initiation and elongation were detected by using labeled antigen-binding fragments on an array of the GR integrated in the genome. Single live-cell imaging showed that H3K27ac favors the recruitment of the TF GR and accelerates the escape of RNAP II from the promoter.

The above publications were designed to achieve different goals. While the work done on the *GAL* genes offers a better spatial resolution on chromatin structure, the study on the GR offers a better time resolution of the events that lead to efficient transcription. The discrepancies

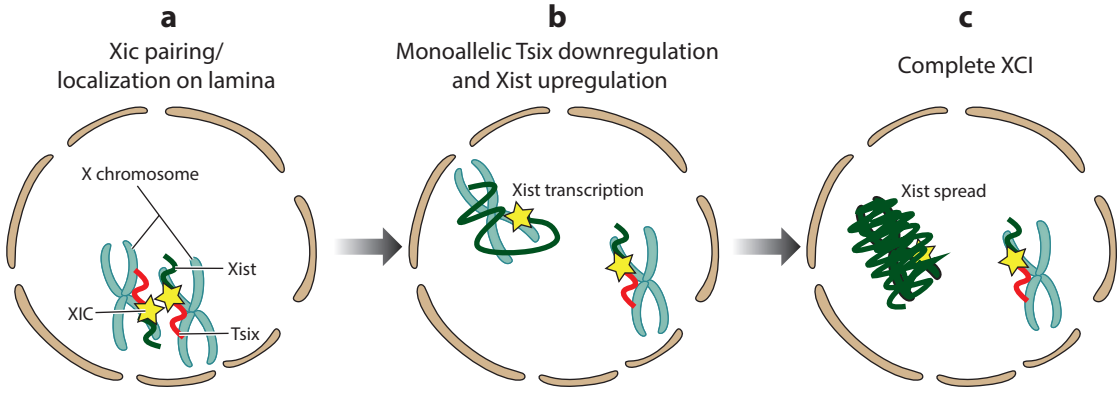

Figure 3

Molecular mechanisms in X chromosome inactivation (XCI) characterized by live imaging approaches. (*a*) A single-locus DNA labeling approach using the *tet*O/TetR system identified X-inactivation center (Xic) pairing prior to initiation of XCI, suggesting it plays a critical role in the choice of which X chromosome is silenced. (*b*) Using simultaneous detection of X-inactive specific transcript (Xist) and Tsix using RNA fluorescent in situ hybridization (FISH) in fixed cells, the temporal order of chromatin remodeling and transcriptional regulation was determined (95). (*c*) Single-molecule detection of Xist RNA using the MS2–MS2 capsid protein (MCP) (98) or pumilio homology domain (PUM-HD) (99) system also revealed the dynamic nature of Xist long noncoding RNA in coating and inactivating the X chromosome.

between both studies on the role of H3 acetylation on transcription could be explained by the use of different model organisms. It is possible that posttranslational histone modification may be critical to arrange the spatial compaction of chromatin in mammalian cells because their nuclear organization is more complex than that of yeast. Alternatively, the dramatic burst of transcription of the *GAL* genes might be higher than that of the GR and, therefore, more dependent on histone remodelers than modifiers. Finally, the *GAL10* gene antisense strand is transcribed into an ncRNA, which prevents transcriptional leakage under repression conditions (93). Thus, gene transcriptional activity might be differentially influenced by histone modification for transcription of nuclear ncRNAs and chromatin organization. This idea is supported by recent work showing that the establishment of neuronal surface identity depends on an lncRNA that leads to DNA methylation and promotes the choice for clusters of protocadherin alpha genes (94).

4.1.3. X chromosome inactivation. X chromosome inactivation (XCI) provides an important example of the influence of lncRNAs, chromatin remodeling, and nuclear positioning on gene activity (**Figure 3**). In female mammalian cells, only one X chromosome remains active to compensate for chromosome dosage between female (XX) and male (XY) cells. XCI is established during early development and maintained through mitotic cell divisions. Silencing of the X chromosome is achieved by the transcriptional regulation of X-inactive specific transcript (Xist) lncRNA and its antisense transcript Tsix from the X-inactivation center (Xic). Single-locus labeling of X chromosome centers (Xic) using the *tet*O system revealed that homologous pairing events determine which X chromosome will be silenced during differentiation (95). The mobility of both X chromosomes increased prior to XCI in undifferentiated cells, then X chromosomes paired for 45 min. After pairing, the monoallelic downregulation of Tsix induced the upregulation of the Xist, which coated the whole X chromosome, silencing its transcription. It has been suggested that direct association of the X chromosome with nuclear lamina is required for Xist RNA spreading (96); however, the pairing or lamina localization models might be still under debate, since a recent report demonstrated that reducing Xic pairing as well as relocation of the X chromosome to the

nuclear lamina does not influence monoallelic Xist transcription (97). Xist transcription and its spread over the whole inactivating X chromosome territory were visualized in living cells using the MS2-MCP system (98). Xist spread on the X chromosome led to the binding of epigenetic and heterochromatin regulators, culminating in transcriptional silencing of the chromosome. Interestingly, transcription of Xist remains active and is necessary for the turnover of bound Xist transcripts by newly transcribed Xist RNA. Xist RNA has a half-life of 4–6 h and a stable association with the chromosome that depends on the functional tethering of a cofactor enhancer of zeste homolog 2 (99). XCI is one of the best-characterized processes of chromatin regulation; understanding the entire process of XCI may reveal common molecular mechanisms underlying chromatin dynamics and transcriptional regulation.

4.1.4. Formation of transcriptional hubs. Transcription of any gene results from a highly coordinated assembly of multiple components of the transcriptional machinery on the DNA. Advances in both biomolecular labeling strategies with the self-labeling HaloTag dyes (100) and imaging modalities such as LSFM have led to the ability to track the different components of the transcriptional machinery with high precision (101). Quantitative measurements of the residence times of TFs, cofactors or mediators on the DNA, and their binding kinetics (102) have yielded insights into the temporal regulation of how individual components interact with each other and with chromatin.

While these tagging systems work effectively in mammalian cells, attempts to use fluorescent tags or dyes in vivo need further optimization. A recently developed protein tag referred to as the LlamaTag, which directly binds to mature fluorescent proteins, has enabled visualization of rapid changes in TF concentration in live *Drosophila* embryos (103). How dynamic changes in TF concentrations affect the assembly of the transcriptional machinery has been explored both biochemically and by imaging. One hypothesis is that TFs, cofactors or mediators, and RNAP II all contain intrinsically disordered, low-complexity domains. The self-assembling nature of these domains allows them to engage in stable interactions that persist over time to facilitate the formation of transcriptional factories (104–106). Biochemical characterization of these factories has highlighted that many of their components could result in phase-separated condensates in the nucleus (107). In living cells, a temporally coordinated cluster formation would facilitate cooperative interactions between the different components of the transcription factory in a timely manner, thereby leading to a controlled onset of transcription. Simultaneous imaging of RNAP II and a transcriptional mediator showed in real time that both these proteins are incorporated in the same phase-separated condensate, thus indicating its heterotypic nature (104). Although these studies provided high temporal dynamics of the transcriptional hubs, it was not evident how hub formation occurred on certain chromatin domains (see the inset in **Figure 2**). Combined DNA FISH and HaloTag TF imaging revealed the formation of hubs on microsatellite repeat regions (108). However, how these self-assembling hubs or condensates affect transcription from endogenous genes has yet to be shown. Simultaneous imaging of these clusters with tagged loci in the future may provide insights into whether such assembly occurs at active gene loci (i.e., whether actively transcribing genes induce the clustering) or the clustering induces the transcription. Further biological relevance of these hubs can be extended toward understanding whether the formation of clusters or condensates changes, especially on inducible genes, which are triggered by external stimuli.

One such example is genes encoding for different heat shock proteins (HSPs), which coalesce into discrete spots in the yeast nucleus upon transcription stimulation. Interallelic clustering in haploid yeast cells was measured as colocalization of different loci labeled with different repeats of the *lac*O/LacI-GFP system (109). The interaction between the HSP104 and HSP12 loci was

dependent on transcriptional activation because mutations on the TATA box abolished it. This result, and the failure of constitutive genes to coalesce, suggested that specific transcriptional factories are formed in response to environmental stimuli and coregulated by unique TFs, such as heat shock factor 1 (109). It remains to be determined if colocalization of HSP genes upon thermal stress is conserved in other organisms with different nuclear organization. In cultured mammalian fibroblasts, different alleles of HSP70 did not coalesce upon transcriptional activation under thermal stress (110); rather, the locus moved from the nuclear periphery to speckles (111). The movement was dependent on nuclear actin polymerization, and its inhibition prevented transcriptional activation as measured with the MS2-MCP system. Therefore, transcription depended on the contact of the gene with nuclear speckles that might serve as transcriptional hubs to tether HSP70 and probably other genes (19). Further evidence that the location of the genes matters was provided by a study in which double-stranded breaks were introduced at two distinct chromatin locations: a promoter-proximal region downstream of the transcription start site and a region within an internal exon (intergenic region) (112). Transcription from these locations after induction of double-stranded DNA breaks was monitored with two reporter constructs, using MS2 tagging, PP7 tagging, or both. While suppression of preexisting transcription occurred after such breaks, damage at the intergenic regions resulted in transcriptional recovery. This site-specific transcriptional recovery was possibly due to local nucleosome depletion, highlighting the importance of chromatin regions influencing DNA damage–induced transcriptional responses.

The recent advances in labeling of DNA loci with CRISPR-Cas9 and tagging endogenous genes in various organisms have provided insights into the dynamic changes in the nuclear architecture and the assembly of transcriptional factories, as well as how these changes regulate transcription.

4.2. Transcription Dynamics: Initiation and Elongation

Transcription kinetics with high temporal sensitivity have been determined with technologies to tag endogenous genes using the CRISPR-Cas9 system and fluorescent tags for labeling mRNAs. Transcription initiation occurs in an irregular stochastic fashion, in which a period of transcriptional activity is followed by an inactive period. This leads to the well-established random telegraph model (113) in which stochastic switching between transcriptionally inactive and active states is referred to as bursts. Transcriptional bursting is one of the underlying components of gene expression noise and the heterogeneity observed between genetically identical cells. Based on the nature of the bursting behavior, one can begin to infer the molecular regulation of bursting, which is often unique to each gene and even each allele. Some of the key parameters analyzed are amplitude (the intensity of transcription), frequency (how often bursts occur), and duration (how long bursts persist). While these analyses provide insights into transcriptional regulation, more detailed understanding requires mathematical models incorporating different promoter states. Several studies have shown that transcription initiation is a multistep process, and promoters often fluctuate in different timescales in different organisms. This has been described in other reviews (e.g., 36, 113).

Besides tracking transcription from single genes, the use of orthogonal tags such as MS2 and PP7 has furthered our understanding of how multiple genes behave with respect to each other in their native state. This was best exemplified by a study that measured transcription from two distinct MS2- and PP7-labeled genes in *Drosophila* embryos that are controlled by the same *snail* shadow enhancer. When the enhancer was placed equidistant from MS2 and PP7 reporter genes in a symmetric orientation, similar bursting frequencies of both reporters were observed. However, when the enhancer was placed closer to the PP7 reporter, sustained transcription was observed

from the PP7 locus, with a significant increase in burst frequency compared to the MS2 reporter (88). These results showed that competition between genes for the same enhancer can modulate bursting frequencies. Recent evidence using reporter constructs and endogenous genes has highlighted how histone modifications can also play a role in modulating bursting frequencies. For example, transcriptional bursting of a luciferase reporter controlled by a circadian gene promoter revealed that the burst frequency was modulated by the circadian time, whereas the burst size was determined by the site of integration. The circadian changes are correlated with the histone acetylation levels, and CRISPR-Cas9-mediated acetylation of the promoter was sufficient to change the burst frequency (114). Such regulation of burst frequency but not burst size by acetylating histones has been shown for inducible genes such as *c-fos* from fixed cell studies (115). Based on both fixed-cell and live imaging studies, the burst size appears to be modulated primarily by the kinetics of the TF binding (49, 116), whereas the histone modifications impact the burst frequency.

Along with transcription initiation, direct measurements of the dynamics of transcription elongation in single cells have been made possible by positioning the MS2 and PP7 stem-loops in the 5′ and 3′ ends of the same gene. By ensuring that the nucleotide sequence between the two labels was sufficiently long, researchers were able to use the time between the appearance of the 5′ and 3′ labels to directly measure RNAP II elongation rates (1). Using a reporter gene in yeast in which Midasin AAA ATPase 1 (*MDN1*) is driven by the *GAL* promoter, the average RNAP II elongation rate was measured at 25 ± 2 bases/s upon galactose induction. Significant cell-to-cell heterogeneity was observed in the measured elongation rates, which varied widely across organisms. A similar experimental design in *Drosophila* embryos yielded an average elongation rate of 40 bases/s, and this was independent of the TF gradients along the anterior–posterior axis of the embryos. Interestingly, when a ponasterone A inducible promoter was used in cancer U2OS cells and the stem-loop cassettes were placed 3 kb apart, RNAP II elongation rates were measured to be much faster, at 100 bases/s. The different elongation rates may arise owing to the differences in the reporter designs and the genomic environment where the integration of the reporter occurs or, alternatively, stochastic pausing of polymerases. Utilizing strategies such as reporter genes with both MS2 and PP7 integrated at a specific locus with varying promoters, as performed in yeast (117), would help decouple the contribution of the promoter and the genomic environment from the *trans*-regulatory elements in determining elongation rates. In the future, insertion of the stem-loops in the 5′ and 3′ ends of the endogenous genes will further validate whether these measurements are affected by *cis*- or *trans*-regulatory elements of the genome.

Transcription dynamics mark the beginning of the extensive regulation of gene expression. The posttranscriptional processing of the nascent transcripts, cytoplasmic export and localization, and their translational status determine the fate of these transcripts.

5. RNA PROCESSING AND LOCALIZATION

One property common to many cellular RNAs is that they are posttranscriptionally modified. This processing affects the subcellular localization and fate of RNAs and can be rapidly modified to regulate gene expression in response to environmental changes. Imaging posttranscriptional events occurring both in the nucleus and in the cytoplasm has characterized the life cycle of mRNAs with high temporal resolution, and several reviews have described each step in the life cycle of single mRNAs in great detail (36–38, 118, 119). To summarize, cotranscriptional pre-mRNA splicing in living cells was visualized by labeling introns using either the MS2 system (120–122) or MBs (123). Frequencies of splicing monitored at single transcriptional sites revealed stochasticity of co- and posttranscriptional splicing (122) and differential splicing kinetics between two introns in the same transcript (120). The dynamics of single-mRNA nucleocytoplasmic export through nuclear pores

have been investigated using several approaches. With the MS2-MCP system, either rapid export of mRNPs (0.5 s) (124) or a three-step process including docking, transport, and release (durations of approximately 80, 5–20, and 80 ms, respectively) was characterized (40). Three-dimensional export routes and selectivity mechanisms were addressed with single-point edge-excitation subdiffraction microscopy (125). Interestingly, approximately 36% of mRNP molecules that encountered the nuclear pore successfully completed export. In a study using LSFM, approximately 25% of mRNP molecules exported rapidly after encountering the nuclear envelope (from 65 ms to up to several seconds) in *Chironomus tentans* (126). The functional association of the mRNA export factor nuclear RNA export factor 1 (NXF1) with the cytoplasmic side of the nuclear pore was identified using real-time single-molecule mRNA tracking as well as stimulated emission depletion superresolution microscopy and fluorescence lifetime imaging microscopy–FRET in fixed cells (127). Live imaging of PP7-labeled mRNAs in yeast indicated that once the RNA reaches the nuclear periphery, it is not immediately exported. Instead, mRNAs scan the nuclear periphery until they find a nuclear pore that enables their export. The scanning behavior is influenced by the nuclear basket proteins myosin-like protein 1 and 2 (MLP1/2) and the nuclear abundant poly(A) RNA-binding protein 2 (Nab2) (128). Once exported into the cytoplasm, these mRNPs may undergo a dynamic exchange of RNA-binding proteins, translate immediately, or localize to subcellular compartments to be translated in response to specific cues. In this section, we discuss the recent advances in imaging that allow us to follow the fate of mRNAs from RNA localization to translation to decay, as well as the less explored journey of ncRNAs.

5.1. Localization of Noncoding RNA

ncRNAs are functional RNA transcripts that play fundamental roles in a broad variety of cellular processes. They are categorized into two types: small (<30 nucleotides) and long (>200 nucleotides). Live imaging of some nuclear lncRNAs, such as Xist and TERRA, and their function in nuclear organization and chromatin dynamics have been reviewed in Sections 3 and 4.1.3. Small ncRNAs include transfer RNAs (tRNAs), microRNAs (miRNAs), small interfering RNAs (siRNAs), Piwi-interacting RNAs (piRNAs), small nucleolar RNAs (snoRNAs), and the spliceosomal small ncRNPs. Single-molecule imaging of small ncRNAs is precluded by the difficulty of multimerizing fluorophores in such a small molecule without perturbing its function and maturation.

High-resolution single-molecule approaches could reveal a great deal about the complex life cycle of splicing factors and how miRNA binding kinetics affect the fate of mRNAs. Unperturbed tagging of the splicing factor U1 small nuclear RNA has been possible with the Riboglow system (55) (**Table 1**). This system enabled visualization of U1 small nuclear RNP localization in Cajal bodies in the nucleus and in U bodies in the cytoplasm upon stress induction. Nonetheless, it was not powerful enough to track single U1 molecules and investigate the impact of stress on its maturation process. Regarding the regulation of mRNAs by the binding of miRNAs, a recent imaging approach attempted to answer how the low copy number of miRNA could regulate a specific mRNA target (129). It was hypothesized that specificity depended on the spatial proximity between miRNA and mRNA. Using a probe with a fluorophore and a quencher, a fluorogenic system was designed that reported on miRNA maturation. The binding of the probe to the pre-miRNA allowed the quencher to be removed after dicer processing and the fluorophore to remain bound and reveal the mature miRNA. This conferred high specificity and low background, enabling visualization of miRNA maturation after local stimulation of neuronal dendrites (129). The functional impact of miRNA was measured by inhibition of translation of the mRNA targets that localized in the same dendrite. It remains to be determined if the target specificity observed in neurons is cell type– or miRNA-dependent.

5.2. Link Between Localization and mRNA Translation

The sophisticated interplay of *cis*- and *trans*-regulatory elements in the mRNA life cycle determines where and when an mRNA will be translated. Local mRNA translation plays a crucial role in highly regulated processes such as embryo development in *Drosophila* (44), synapse formation in stimulated dendrites in neurons (extensively reviewed by 118 and 130–132), and cell cycle progression in the budding yeast *S. cerevisiae* (133). The generally accepted model is that mRNAs travel in a translationally repressed state to the specific location in the cell where protein is needed. This has been well exemplified during mRNA transport along microtubules in neurons, during which β-actin mRNAs bound by ZBP1 are packed in granules until local activity unmasks these mRNAs for translation (39). The cycle of unmasking and remasking takes about 15 min. Active transport of mRNAs is regulated by *cis* and *trans* factors, which influence how they associate with the motor proteins to travel along microtubule tracks (reviewed in 118). A recent study has identified a new mode of transportation of the RNA granules, showing that they hitchhike on lysosomes in mammalian cells during axonal transport in primary neurons (134). Annexin A11 tethers β-actin mRNA–containing granules to lysosomes by means of phase-separation and membrane-binding properties of its N- and C-terminal regions, respectively (134). In neurons, transport of mRNAs to distal regions by docking on lysosomes may have implications in cellular homeostasis. In the case of Rgs4 mRNA, its 3′ UTR fine-tunes the direct transport of the mRNA to dendrites and its association with synapses (135).

Besides mRNAs and RNA-binding proteins, translation factors are often packaged in complexes with mRNAs, which are transported to sites of action. In migrating mouse embryonic fibroblasts, simultaneous imaging and cotracking of single β-actin mRNAs using the MS2 system and ribosomes labeled with photoactivatable fluorescence proteins revealed active translation at focal adhesions, resulting in reduced mRNA diffusion speeds (136). However, not all mRNAs are locally translated to influence migration in fibroblasts. For example, adenomatous polyposis coli–dependent mRNAs are globally translated in the cell, and they undergo translational silencing by granule formation at sites of protrusion retraction (137). In yeast, specific granules harboring the mRNAs of translation factors, also known as translation factories, are transported to the bud tip (138). Localization of the translation factories in the bud tip is myosin dependent and relies on the RNA-binding protein She2 and the scaffold protein She3. To visualize how mRNA transport and local translation are coupled in all these cell types, dual labeling of mRNA with MS2 and PP7 aptamers and the nascent peptides with the SunTag system will be extremely informative. SunTag is a series of the GCN4 epitope that is genetically integrated in the 5′ end of the coding sequence of the mRNA of interest (139). Ongoing translation kinetics are assessed by the rapid binding of fluorescently tagged single-chain antibody fragments that recognize the GCN4 epitope as soon as it is translated in the cell (43, 140–143). Since the GCN4 epitope is derived from yeast, a modified SunTag system will be required for translation kinetics there. New versions of epitopes that can report nascent protein synthesis have been developed (144–146).

The unifying theme obtained from mRNA transport in various organisms is that functionality is achieved by confining the regulator and its molecular targets in the same cellular location. In one specific situation, this consensus is challenged: the localization of mRNAs with ncRNAs, translation factors, and decay enzymes in SGs and processing bodies (PBs) during the stress response. The recruitment of mRNAs to SGs and PBs in the cytoplasm is a dynamic process. Different mRNAs show different residency times in these biomolecular condensates and competence to traffic back and forth between these condensates and the cytoplasm (42, 147). The translation status of these mRNAs was assessed using the SunTag system, which showed that mRNAs cease translation prior to entry into SGs and resume translation rapidly once SGs have been dissolved (11, 12). Hence,

the recruitment of mRNAs to SGs and PBs might provide a protection mechanism for mRNAs during stress and the means for a rapid restart of translation once the stress ceases (42, 147).

Localization of RNAs in specific sites of the cell is a conserved and dynamic process regulated by *cis* and *trans* elements. It provides the cell with the plasticity to express proteins in response to internal requirements and external cues. Efficiency of mRNA translation can also influence the decay of the mRNA.

5.3. mRNA Turnover

Capturing the dynamics of mRNA degradation at single-molecule resolution has been technically challenging. The initial MS2-MCP system generated fluorescent degradation intermediates due to the high-affinity binding of MCP to MS2, which could not be displaced by the mRNA degradation machinery in yeast (45–48). This problem was resolved by generating a version of the MS2 system that degrades simultaneously with the coding sequence (45). Imaging challenges have yet to be overcome to quantify mRNA degradation accurately. One technical limitation is the measurement of mRNA degradation as the result of the disappearance of the fluorescent signal emitted by single mRNA molecules. The fast cytosolic diffusion of mRNAs makes it difficult to distinguish degradation from the loss of signal caused by free molecular diffusion into out-of-focus *z*-planes. Multifocal imaging could compensate for this molecular diffusion, but in turn, it causes signal loss due to rapid photobleaching. Two independent solutions have been found to circumvent these problems and answer two unrelated questions on decay. The first solution, known as the 3′-RNA end accumulation during turnover (TREAT) system, was used to study the fate of the mRNAs in PBs (42) (**Figure 4*b, i***). The system arose from the two-color labeling method using PP7 and MS2 stem-loops, which was originally reported as a translation detection tool known as translating RNA imaging by coat protein knockoff (TRICK) (44) (**Figure 4*a, i***). In the TRICK system, translated mRNAs can be distinguished from untranslated mRNAs by the displacement of fluorescence-PP7 labeling on the open reading frame by an elongating ribosome. For TREAT, instead of inserting the PP7 stem-loops in an open reading frame, each mRNA is tagged in its 3′ UTR with the MS2 and PP7 systems separated by a viral pseudoknot that inhibits degradation by the enzyme 5′-3′ exoribonuclease 1. Intact mRNAs are detected by both MS2 and PP7 signals, and upon degradation, the decay fragments carrying the pseudoknots are easily identified by the exclusive detection of the signal from the PP7-PCP system. The conversion of an mRNA from two-color to a single color provides a highly quantitative detection system of mRNA degradation.

The second solution is an mRNA tethering system. It has been successfully used to investigate the dynamics of nonsense-mediated decay (NMD). NMD is an mRNA surveillance mechanism that cleaves mRNAs containing premature termination codons (PTCs) in a translation-dependent manner and therefore limits the production of truncated proteins. NMD on single mRNAs was visualized in real time by tagging mRNAs in their 3′ UTR with PP7 and tethering them to the plasma membrane with the CAAX-PCP system to prevent their diffusion (41) (**Figure 4*b, ii***). The reporter mRNA containing the PTC also encoded the SunTag translation detection system in the N terminus (43, 139, 141–143). The SunTag signal provided the means to assess the probability of a ribosome triggering NMD as measured by the separation of the SunTag and PP7 fluorescent signals caused by endonucleolytic cleavage during NMD (148). Since the separation events of the SunTag and PP7 fluorescent signals can also represent the peptide release from translation termination at PTC, the authors accounted for the moment of the 3′ end decay by measuring the vanishing of the PP7-PCP signal (**Figure 4*b, ii***). Simultaneous detection of the SunTag and PP7 signals suggests that not only the first ribosome but each ribosome that terminates translation at the PTC has an equal probability of triggering NMD. Also, the efficiency of NMD was

influenced by the exon sequence downstream of the PTC and the PTC-to-intron distance. Given that most PTC-containing mRNAs are expected to be degraded immediately after mRNA export before reaching the plasma membrane (149), CAAX-tethered mRNA molecules used to study NMD might be selectively capturing mRNA molecules that have escaped from or were subjected

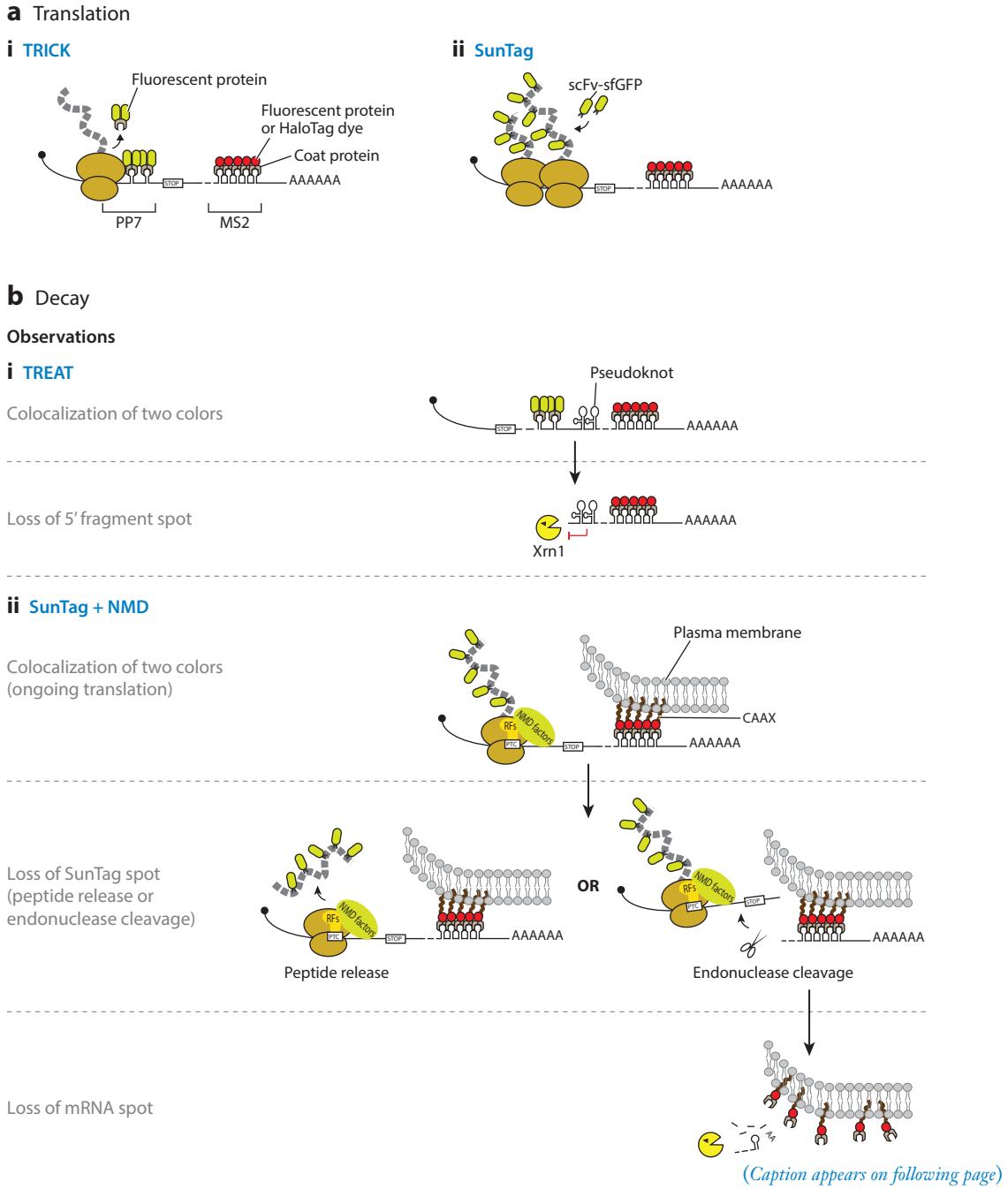

(*Caption appears on following page*)

Figure 4 (*Figure appears on preceding page*)

Fluorescent imaging approaches to detect translation and mRNA decay in living cells. (*a*) Live-cell imaging of translation on single-molecule mRNA. (*i*) Translating mRNA imaging by coat protein knockoff (TRICK). By measuring the displacement of fluorescence-PP7 labeling from open reading frames on reporter mRNA by the first elongating ribosome, this imaging method distinguishes translated from untranslated mRNA (44). (*ii*) Nascent peptide detection of translating ribosomes using the SunTag system. The nascent peptides of SunTag are labeled with superfolder GFP (sfGFP)-tagged single-chain variable fragment (scFv-sfGFP) on translating mRNAs (43, 143–146). (*b*) Live-cell imaging of single mRNA decay. (*i*) 3′-RNA end accumulation during turnover (TREAT): Similar to the two-color labeling scheme of TRICK, but both PP7 and MS2 stem-loops are located in the 3′ untranslated region. Pseudoknots are inserted between PP7 and MS2 stem-loops to distinguish the decay fragment (one color) from intact mRNA (two color) (42). (*ii*) Nonsense-mediated decay (NMD) reporter with the SunTag system. The combination of the SunTag translational reporter system and CAAX-tethered mRNA allows one to monitor the translation kinetics of NMD (41). Normal termination codons (STOPs), premature termination codons (PTCs), and release factors (RFs) are shown.

to slow NMD. However, the tethering approach offers an attractive benefit to track the moment of mRNA decay in living cells. Using these imaging tools, it is now possible to determine the kinetics of mRNA decay and the sequence specificity of this process (whether the efficiency of the decay of 3′ end regions is sequence dependent or whether some sequences can escape degradation). Recent publications suggested that sequences of PTC-containing mRNA could participate in a genetic compensation response (150, 151). Identifying and imaging the behavior of these RNAs will provide insights into the feedback loop described for mRNA decay on transcriptional regulation and even nuclear organization.

6. CONCLUSIONS AND PERSPECTIVE

Simultaneous imaging of specific DNA loci and RNA is providing a fresh perspective on how temporal coordination between different events, from DNA replication to transcription to mRNA processing, translation, and decay, is attained despite stochasticity at every step. Imaging living cells in action at the single-molecule level is opening new venues to explore chromatin dynamics and RNA functions that influence gene expression and go beyond the synthesis of proteins. It provides the means to track these molecules and answer when and where their actions influence the functional events in a cell. These observations pave the way for researchers to design multicolor imaging experiments and determine how several factors efficiently interact. For example, the simultaneous imaging of specific nuclear components, such as mediators, enhancers, and nascent RNAs, affords a way to distinguish productive intermolecular interactions from spurious ones as a function of time and to determine how this contributes to restructuring the nuclear architecture for genetic decisions. Visualizing the temporal order of their interactions will also define the factors and events that facilitate or fine-tune cellular processes. Therefore, it is necessary to choose the factors that need to be tagged and quantify their behavior in living cells to characterize the events that ultimately define cell fate and functionality.

Two goals for the future of the single-molecule live imaging field are multiplexed imaging of several factors to understand their temporal dynamics relative to each other and the study of cellular processes in whole organisms. Several efforts are being made to take on the challenge of simultaneously visualizing more than three components involved in a cellular action at a high imaging speed without photobleaching or photodamaging the sample. A palette of a new generation of brighter, more photostable fluorescent dyes has been introduced. The photoactivatable and photoconvertible versions, such as the new Janelia Fluorophore HaloTag dyes, provide greater localization precision (152, 153). Faster and more sensitive microscopy techniques, including LSFM for 3D imaging, allow one to localize single particles with high sensitivity with minimal phototoxic damage to cells (154, 155). New algorithms to analyze and provide statistics from the data generated by imaging approaches are constantly being developed (156). Although

advanced imaging technologies have expanded our approaches for visualizing the various steps of gene expression with high temporal and spatial resolution, the widespread use of these technologies has been technically challenging in intact tissue and whole organisms. Most labeling schemes for single-molecule approaches rely on insertion of multiple repeat sequences such as stem-loops or binding motifs and multimerization of the fluorescent proteins, which raises concerns about the genetic manipulations of the native DNA sequences or loading the RNAs with bulky fluorescent molecules. This also poses significant challenges for labeling small nucleic acids such as ncRNAs and miRNAs and imaging them as single molecules over long periods of time. To address these concerns, we foresee that DNA and RNA imaging systems based on nongenetic tagging need to be optimized for brightness and specificity to allow detection of endogenous molecules in the physiological context of tissue and live animals. These advances are needed to investigate the structure and organization of the nucleus, the communication between the nucleus and the cytoplasm, and the role of biomolecular condensates in cells when functioning in their tissue microenvironment. Other fields that will certainly benefit from these technologies are cytogenetic diagnosis (33) in primary cells and RNA therapeutics. Localizing the therapeutic RNA molecules and following them over time in their physiologically relevant environment will enable fine-tuning of therapeutically administered dosages.

A dynamic cellular environment provides the plasticity for meaningful interactions, some of which can influence the steps of chromatin organization and gene expression. To decipher the functional cellular network, further development of novel tagging systems, not just limited to fluorescent proteins, is required for multiplex detection of the different components at various steps of the life cycle of DNA and RNA. This future era of technological revolution requires integration of the findings of single-molecule fluorescence microscopy with biochemical approaches that offer a complementary perspective on the interactions and localization of a molecule during its life.

DISCLOSURE STATEMENT

The authors are not aware of any affiliations, memberships, funding, or financial holdings that might be perceived as affecting the objectivity of this review.

ACKNOWLEDGMENTS

We apologize to the authors of the articles we did not cite because of space limitations. This work has been completed with funding from US National Institutes of Health (NIH) grants NS083085, GM57071, and 5U01DA047729 to R.H.S. and NIH grant AG05583 and Natural Sciences and Engineering Research Council of Canada grant RGPIN-2019-04767 to M.V.

LITERATURE CITED

1. Hocine S, Raymond P, Zenklusen D, Chao JA, Singer RH. 2013. Single-molecule analysis of gene expression using two-color RNA labeling in live yeast. *Nat. Methods* 10:119–21
2. Larson DR, Zenklusen D, Wu B, Chao JA, Singer RH. 2011. Real-time observation of transcription initiation and elongation on an endogenous yeast gene. *Science* 332:475–78
3. Shav-Tal Y, Darzacq X, Singer RH. 2006. Gene expression within a dynamic nuclear landscape. *EMBO J.* 25:3469–79
4. Fukaya T, Lim B, Levine M. 2016. Enhancer control of transcriptional bursting. *Cell* 166:358–68
5. Garcia HG, Tikhonov M, Lin A, Gregor T. 2013. Quantitative imaging of transcription in living *Drosophila* embryos links polymerase activity to patterning. *Curr. Biol.* 23:2140–45
6. McSwiggen DT, Mir M, Darzacq X, Tjian R. 2019. Evaluating phase separation in live cells: diagnosis, caveats, and functional consequences. *Genes Dev.* 33:1619–34

7. Snead WT, Gladfelter AS. 2019. The control centers of biomolecular phase separation: how membrane surfaces, PTMs, and active processes regulate condensation. *Mol. Cell* 76:295–305
8. Mir M, Stadler MR, Ortiz SA, Hannon CE, Harrison MM, et al. 2018. Dynamic multifactor hubs interact transiently with sites of active transcription in *Drosophila* embryos. *eLife* 7:e40497
9. Tsai A, Alves MR, Crocker J. 2019. Multi-enhancer transcriptional hubs confer phenotypic robustness. *eLife* 8:e45325
10. Guzikowski AR, Chen YS, Zid BM. 2019. Stress-induced mRNP granules: form and function of processing bodies and stress granules. *Wiley Interdiscip. Rev. RNA* 10:e1524
11. Moon SL, Morisaki T, Khong A, Lyon K, Parker R, Stasevich TJ. 2019. Multicolour single-molecule tracking of mRNA interactions with RNP granules. *Nat. Cell Biol.* 21:162–68
12. Wilbertz JH, Voigt F, Horvathova I, Roth G, Zhan Y, Chao JA. 2019. Single-molecule imaging of mRNA localization and regulation during the integrated stress response. *Mol. Cell* 73:946–58.e7
13. Jalihal AP, Lund PE, Walter NG. 2019. Coming together: RNAs and proteins assemble under the single-molecule fluorescence microscope. *Cold Spring Harb. Perspect. Biol.* 11:a032441
14. Daetwyler S, Huisken J. 2016. Fast fluorescence microscopy with light sheets. *Biol. Bull.* 231:14–25
15. Chen BC, Legant WR, Wang K, Shao L, Milkie DE, et al. 2014. Lattice light-sheet microscopy: imaging molecules to embryos at high spatiotemporal resolution. *Science* 346:1257998
16. Robinett CC, Straight A, Li G, Willhelm C, Sudlow G, et al. 1996. In vivo localization of DNA sequences and visualization of large-scale chromatin organization using lac operator/repressor recognition. *J. Cell Biol.* 135:1685–700
17. Ding DQ, Hiraoka Y. 2017. Visualization of a specific genome locus by the *lacO*/LacI-GFP system. *Cold Spring Harb. Protoc.* 2017:pdb.prot091934
18. Belmont AS. 2001. Visualizing chromosome dynamics with GFP. *Trends Cell Biol.* 11:250–57
19. Tasan I, Sustackova G, Zhang L, Kim J, Sivaguru M, et al. 2018. CRISPR/Cas9-mediated knock-in of an optimized TetO repeat for live cell imaging of endogenous loci. *Nucleic Acids Res.* 46:e100
20. Fu Y, Rocha PP, Luo VM, Raviram R, Deng Y, et al. 2016. CRISPR-dCas9 and sgRNA scaffolds enable dual-colour live imaging of satellite sequences and repeat-enriched individual loci. *Nat. Commun.* 7:11707
21. Ma H, Reyes-Gutierrez P, Pederson T. 2013. Visualization of repetitive DNA sequences in human chromosomes with transcription activator-like effectors. *PNAS* 110:21048–53
22. Ma Y, Wang M, Li W, Zhang Z, Zhang X, et al. 2017. Live cell imaging of single genomic loci with quantum dot-labeled TALEs. *Nat. Commun.* 8:15318
23. Lindhout BI, Fransz P, Tessadori F, Meckel T, Hooykaas PJ, van der Zaal BJ. 2007. Live cell imaging of repetitive DNA sequences via GFP-tagged polydactyl zinc finger proteins. *Nucleic Acids Res.* 35:e107
24. Lane AB, Strzelecka M, Ettinger A, Grenfell AW, Wittmann T, Heald R. 2015. Enzymatically generated CRISPR libraries for genome labeling and screening. *Dev. Cell* 34:373–78
25. Chen B, Gilbert LA, Cimini BA, Schnitzbauer J, Zhang W, et al. 2013. Dynamic imaging of genomic loci in living human cells by an optimized CRISPR/Cas system. *Cell* 155:1479–91
26. Chen B, Guan J, Huang B. 2016. Imaging specific genomic DNA in living cells. *Annu. Rev. Biophys.* 45:1–23
27. Qin P, Parlak M, Kuscu C, Bandaria J, Mir M, et al. 2017. Live cell imaging of low- and non-repetitive chromosome loci using CRISPR-Cas9. *Nat. Commun.* 8:14725
28. Ma H, Naseri A, Reyes-Gutierrez P, Wolfe SA, Zhang S, Pederson T. 2015. Multicolor CRISPR labeling of chromosomal loci in human cells. *PNAS* 112:3002–7
29. Ma H, Tu LC, Naseri A, Huisman M, Zhang S, et al. 2016. Multiplexed labeling of genomic loci with dCas9 and engineered sgRNAs using CRISPRainbow. *Nat. Biotechnol.* 34:528–30
30. Ma H, Tu LC, Naseri A, Chung YC, Grunwald D, et al. 2018. CRISPR-Sirius: RNA scaffolds for signal amplification in genome imaging. *Nat. Methods* 15:928–31
31. Wu X, Mao S, Yang Y, Rushdi MN, Krueger CJ, Chen AK. 2018. A CRISPR/molecular beacon hybrid system for live-cell genomic imaging. *Nucleic Acids Res.* 46:e80
32. Mao S, Ying Y, Wu X, Krueger CJ, Chen AK. 2019. CRISPR/dual-FRET molecular beacon for sensitive live-cell imaging of non-repetitive genomic loci. *Nucleic Acids Res.* 47:e131

33. Wang H, Nakamura M, Abbott TR, Zhao D, Luo K, et al. 2019. CRISPR-mediated live imaging of genome editing and transcription. *Science* 365:1301–5
34. Bertrand E, Chartrand P, Schaefer M, Shenoy SM, Singer RH, Long RM. 1998. Localization of *ASH1* mRNA particles in living yeast. *Mol. Cell* 2:437–45
35. Wu B, Chao JA, Singer RH. 2012. Fluorescence fluctuation spectroscopy enables quantitative imaging of single mRNAs in living cells. *Biophys. J.* 102:2936–44
36. Pichon X, Lagha M, Mueller F, Bertrand E. 2018. A growing toolbox to image gene expression in single cells: sensitive approaches for demanding challenges. *Mol. Cell* 71:468–80
37. Tutucci E, Livingston NM, Singer RH, Wu B. 2018. Imaging mRNA in vivo, from birth to death. *Annu. Rev. Biophys.* 47:85–106
38. Vera M, Biswas J, Senecal A, Singer RH, Park HY. 2016. Single-cell and single-molecule analysis of gene expression regulation. *Annu. Rev. Genet.* 50:267–91
39. Buxbaum AR, Wu B, Singer RH. 2014. Single β-actin mRNA detection in neurons reveals a mechanism for regulating its translatability. *Science* 343:419–22
40. Grunwald D, Singer RH. 2010. In vivo imaging of labelled endogenous β-actin mRNA during nucleocytoplasmic transport. *Nature* 467:604–7
41. Hoek TA, Khuperkar D, Lindeboom RGH, Sonneveld S, Verhagen BMP, et al. 2019. Single-molecule imaging uncovers rules governing nonsense-mediated mRNA decay. *Mol. Cell* 75:324–39.e11
42. Horvathova I, Voigt F, Kotrys AV, Zhan Y, Artus-Revel CG, et al. 2017. The dynamics of mRNA turnover revealed by single-molecule imaging in single cells. *Mol. Cell* 68:615–25.e9
43. Wu B, Eliscovich C, Yoon YJ, Singer RH. 2016. Translation dynamics of single mRNAs in live cells and neurons. *Science* 352:1430–35
44. Halstead JM, Lionnet T, Wilbertz JH, Wippich F, Ephrussi A, et al. 2015. An RNA biosensor for imaging the first round of translation from single cells to living animals. *Science* 347:1367–71
45. Tutucci E, Vera M, Biswas J, Garcia J, Parker R, Singer RH. 2018. An improved MS2 system for accurate reporting of the mRNA life cycle. *Nat. Methods* 15:81–89
46. Garcia JF, Parker R. 2015. MS2 coat proteins bound to yeast mRNAs block 5′ to 3′ degradation and trap mRNA decay products: implications for the localization of mRNAs by MS2-MCP system. *RNA* 21:1393–95
47. Garcia JF, Parker R. 2016. Ubiquitous accumulation of 3′ mRNA decay fragments in *Saccharomyces cerevisiae* mRNAs with chromosomally integrated MS2 arrays. *RNA* 22:657–59
48. Haimovich G, Zabezhinsky D, Haas B, Slobodin B, Purushothaman P, et al. 2016. Use of the MS2 aptamer and coat protein for RNA localization in yeast: a response to "MS2 coat proteins bound to yeast mRNAs block 5′ to 3′ degradation and trap mRNA decay products: implications for the localization of mRNAs by MS2-MCP system." *RNA* 22:660–66
49. Das S, Moon HC, Singer RH, Park HY. 2018. A transgenic mouse for imaging activity-dependent dynamics of endogenous Arc mRNA in live neurons. *Sci. Adv.* 4:eaar3448
50. Lionnet T, Czaplinski K, Darzacq X, Shav-Tal Y, Wells AL, et al. 2011. A transgenic mouse for in vivo detection of endogenous labeled mRNA. *Nat. Methods* 8:165–70
51. Park HY, Lim H, Yoon YJ, Follenzi A, Nwokafor C, et al. 2014. Visualization of dynamics of single endogenous mRNA labeled in live mouse. *Science* 343:422–24
52. Paige JS, Wu KY, Jaffrey SR. 2011. RNA mimics of green fluorescent protein. *Science* 333:642–46
53. Filonov GS, Moon JD, Svensen N, Jaffrey SR. 2014. Broccoli: rapid selection of an RNA mimic of green fluorescent protein by fluorescence-based selection and directed evolution. *J. Am. Chem. Soc.* 136:16299–308
54. Autour A, Jeng SCY, Cawte AD, Abdolahzadeh A, Galli A, et al. 2018. Fluorogenic RNA Mango aptamers for imaging small non-coding RNAs in mammalian cells. *Nat. Commun.* 9:656
55. Braselmann E, Wierzba AJ, Polaski JT, Chrominski M, Holmes ZE, et al. 2018. A multicolor riboswitch-based platform for imaging of RNA in live mammalian cells. *Nat. Chem. Biol.* 14:964–71
56. Chen X, Zhang D, Su N, Bao B, Xie X, et al. 2019. Visualizing RNA dynamics in live cells with bright and stable fluorescent RNAs. *Nat. Biotechnol.* 37:1287–93

57. Wu J, Zaccara S, Khuperkar D, Kim H, Tanenbaum ME, Jaffrey SR. 2019. Live imaging of mRNA using RNA-stabilized fluorogenic proteins. *Nat. Methods* 16:862–65
58. Tyagi S, Kramer FR. 1996. Molecular beacons: probes that fluoresce upon hybridization. *Nat. Biotechnol.* 14:303–8
59. Chen AK, Davydenko O, Behlke MA, Tsourkas A. 2010. Ratiometric bimolecular beacons for the sensitive detection of RNA in single living cells. *Nucleic Acids Res.* 38:e148
60. Yang Y, Chen M, Krueger CJ, Tsourkas A, Chen AK. 2018. Quantifying gene expression in living cells with ratiometric bimolecular beacons. *Methods Mol. Biol.* 1649:231–42
61. Zhang X, Zajac AL, Huang L, Behlke MA, Tsourkas A. 2014. Imaging the directed transport of single engineered RNA transcripts in real-time using ratiometric bimolecular beacons. *PLOS ONE* 9:e85813
62. Boutorine AS, Novopashina DS, Krasheninina OA, Nozeret K, Venyaminova AG. 2013. Fluorescent probes for nucleic acid visualization in fixed and live cells. *Molecules* 18:15357–97
63. Oomoto I, Suzuki-Hirano A, Umeshima H, Han YW, Yanagisawa H, et al. 2015. ECHO-liveFISH: in vivo RNA labeling reveals dynamic regulation of nuclear RNA foci in living tissues. *Nucleic Acids Res.* 43:e126
64. Yoshimura H. 2018. Live cell imaging of endogenous RNAs using Pumilio homology domain mutants: principles and applications. *Biochemistry* 57:200–8
65. Nelles DA, Fang MY, O'Connell MR, Xu JL, Markmiller SJ, et al. 2016. Programmable RNA tracking in live cells with CRISPR/Cas9. *Cell* 165:488–96
66. Abudayyeh OO, Gootenberg JS, Essletzbichler P, Han S, Joung J, et al. 2017. RNA targeting with CRISPR-Cas13. *Nature* 550:280–84
67. Yuan K, Shermoen AW, O'Farrell PH. 2014. Illuminating DNA replication during *Drosophila* development using TALE-lights. *Curr. Biol.* 24:R144–45
68. Duriez B, Chilaka S, Bercher JF, Hercul E, Prioleau MN. 2019. Replication dynamics of individual loci in single living cells reveal changes in the degree of replication stochasticity through S phase. *Nucleic Acids Res.* 47:5155–69
69. Dovrat D, Dahan D, Sherman S, Tsirkas I, Elia N, Aharoni A. 2018. A live-cell imaging approach for measuring DNA replication rates. *Cell Rep.* 24:252–58
70. Gallardo F, Laterreur N, Cusanelli E, Ouenzar F, Querido E, et al. 2011. Live cell imaging of telomerase RNA dynamics reveals cell cycle-dependent clustering of telomerase at elongating telomeres. *Mol. Cell* 44:819–27
71. Yamada T, Yoshimura H, Shimada R, Hattori M, Eguchi M, et al. 2016. Spatiotemporal analysis with a genetically encoded fluorescent RNA probe reveals TERRA function around telomeres. *Sci. Rep.* 6:38910
72. Avogaro L, Querido E, Dalachi M, Jantsch MF, Chartrand P, Cusanelli E. 2018. Live-cell imaging reveals the dynamics and function of single-telomere TERRA molecules in cancer cells. *RNA Biol.* 15:787–96
73. Cusanelli E, Romero CA, Chartrand P. 2013. Telomeric noncoding RNA TERRA is induced by telomere shortening to nucleate telomerase molecules at short telomeres. *Mol. Cell* 51:780–91
74. Laprade H, Lalonde M, Guerit D, Chartrand P. 2017. Live-cell imaging of budding yeast telomerase RNA and TERRA. *Methods* 114:46–53
75. Gilbert N. 2019. Biophysical regulation of local chromatin structure. *Curr. Opin. Genet. Dev.* 55:66–75
76. Robson MI, Ringel AR, Mundlos S. 2019. Regulatory landscaping: how enhancer-promoter communication is sculpted in 3D. *Mol. Cell* 74:1110–22
77. Lieberman-Aiden E, van Berkum NL, Williams L, Imakaev M, Ragoczy T, et al. 2009. Comprehensive mapping of long-range interactions reveals folding principles of the human genome. *Science* 326:289–93
78. Szabo Q, Bantignies F, Cavalli G. 2019. Principles of genome folding into topologically associating domains. *Sci. Adv.* 5:eaaw1668
79. Fabre PJ, Benke A, Manley S, Duboule D. 2015. Visualizing the *HoxD* gene cluster at the nanoscale level. *Cold Spring Harb. Symp. Quant. Biol.* 80:9–16
80. Bintu B, Mateo LJ, Su JH, Sinnott-Armstrong NA, Parker M, et al. 2018. Super-resolution chromatin tracing reveals domains and cooperative interactions in single cells. *Science* 362:eaau1783

81. Hansen AS, Pustova I, Cattoglio C, Tjian R, Darzacq X. 2017. CTCF and cohesin regulate chromatin loop stability with distinct dynamics. *eLife* 6:e25776
82. Hansen AS, Hsieh TS, Cattoglio C, Pustova I, Saldana-Meyer R, et al. 2019. Distinct classes of chromatin loops revealed by deletion of an RNA-binding region in CTCF. *Mol. Cell* 76:395–411.e13
83. Nagashima R, Hibino K, Ashwin SS, Babokhov M, Fujishiro S, et al. 2019. Single nucleosome imaging reveals loose genome chromatin networks via active RNA polymerase II. *J. Cell Biol.* 218:1511–30
84. Janicki SM, Tsukamoto T, Salghetti SE, Tansey WP, Sachidanandam R, et al. 2004. From silencing to gene expression: real-time analysis in single cells. *Cell* 116:683–98
85. Strom AR, Emelyanov AV, Mir M, Fyodorov DV, Darzacq X, Karpen GH. 2017. Phase separation drives heterochromatin domain formation. *Nature* 547:241–45
86. Larson AG, Elnatan D, Keenen MM, Trnka MJ, Johnston JB, et al. 2017. Liquid droplet formation by HP1α suggests a role for phase separation in heterochromatin. *Nature* 547:236–40
87. Jin F, Li Y, Dixon JR, Selvaraj S, Ye Z, et al. 2013. A high-resolution map of the three-dimensional chromatin interactome in human cells. *Nature* 503:290–94
88. Lim B, Heist T, Levine M, Fukaya T. 2018. Visualization of transvection in living *Drosophila* embryos. *Mol. Cell* 70:287–96.e6
89. Tsai A, Singer RH, Crocker J. 2018. Transvection goes live—visualizing enhancer-promoter communication between chromosomes. *Mol. Cell* 70:195–96
90. Wang H, Xu X, Nguyen CM, Liu Y, Gao Y, et al. 2018. CRISPR-mediated programmable 3D genome positioning and nuclear organization. *Cell* 175:1405–17.e14
91. Dultz E, Mancini R, Polles G, Vallotton P, Alber F, Weis K. 2018. Quantitative imaging of chromatin decompaction in living cells. *Mol. Biol. Cell* 29:1763–77
92. Stasevich TJ, Hayashi-Takanaka Y, Sato Y, Maehara K, Ohkawa Y, et al. 2014. Regulation of RNA polymerase II activation by histone acetylation in single living cells. *Nature* 516:272–75
93. Lenstra TL, Coulon A, Chow CC, Larson DR. 2015. Single-molecule imaging reveals a switch between spurious and functional ncRNA transcription. *Mol. Cell* 60:597–610
94. Canzio D, Nwakeze CL, Horta A, Rajkumar SM, Coffey EL, et al. 2019. Antisense lncRNA transcription mediates DNA demethylation to drive stochastic protocadherin α promoter choice. *Cell* 177:639–53.e15
95. Masui O, Bonnet I, Le Baccon P, Brito I, Pollex T, et al. 2011. Live-cell chromosome dynamics and outcome of X chromosome pairing events during ES cell differentiation. *Cell* 145:447–58
96. Chen CK, Blanco M, Jackson C, Aznauryan E, Ollikainen N, et al. 2016. Xist recruits the X chromosome to the nuclear lamina to enable chromosome-wide silencing. *Science* 354:468–72
97. Pollex T, Heard E. 2019. Nuclear positioning and pairing of X-chromosome inactivation centers are not primary determinants during initiation of random X-inactivation. *Nat. Genet.* 51:285–95
98. Ng K, Daigle N, Bancaud A, Ohhata T, Humphreys P, et al. 2011. A system for imaging the regulatory noncoding *Xist* RNA in living mouse embryonic stem cells. *Mol. Biol. Cell* 22:2634–45
99. Ha N, Lai LT, Chelliah R, Zhen Y, Yi Vanessa SP, et al. 2018. Live-cell imaging and functional dissection of *Xist* RNA reveal mechanisms of X chromosome inactivation and reactivation. *iScience* 8:1–14
100. Grimm JB, Muthusamy AK, Liang Y, Brown TA, Lemon WC, et al. 2017. A general method to fine-tune fluorophores for live-cell and in vivo imaging. *Nat. Methods* 14:987–94
101. Liu Z, Legant WR, Chen BC, Li L, Grimm JB, et al. 2014. 3D imaging of Sox2 enhancer clusters in embryonic stem cells. *eLife* 3:e04236
102. Presman DM, Ball DA, Paakinaho V, Grimm JB, Lavis LD, et al. 2017. Quantifying transcription factor binding dynamics at the single-molecule level in live cells. *Methods* 123:76–88
103. Bothma JP, Norstad MR, Alamos S, Garcia HG. 2018. LlamaTags: a versatile tool to image transcription factor dynamics in live embryos. *Cell* 173:1810–22.e16
104. Cho WK, Spille JH, Hecht M, Lee C, Li C, et al. 2018. Mediator and RNA polymerase II clusters associate in transcription-dependent condensates. *Science* 361:412–15
105. Hnisz D, Shrinivas K, Young RA, Chakraborty AK, Sharp PA. 2017. A phase separation model for transcriptional control. *Cell* 169:13–23

106. Lu H, Yu D, Hansen AS, Ganguly S, Liu R, et al. 2018. Phase-separation mechanism for C-terminal hyperphosphorylation of RNA polymerase II. *Nature* 558:318–23
107. Plys AJ, Kingston RE. 2018. Dynamic condensates activate transcription. *Science* 361:329–30
108. Chong S, Dugast-Darzacq C, Liu Z, Dong P, Dailey GM, et al. 2018. Imaging dynamic and selective low-complexity domain interactions that control gene transcription. *Science* 361:eaar2555
109. Chowdhary S, Kainth AS, Gross DS. 2017. Heat shock protein genes undergo dynamic alteration in their three-dimensional structure and genome organization in response to thermal stress. *Mol. Cell. Biol.* 37:e00292-17. Erratum. 2018. *Mol. Cell. Biol.* 38:e00069-18
110. Vera M, Pani B, Griffiths LA, Muchardt C, Abbott CM, et al. 2014. The translation elongation factor eEF1A1 couples transcription to translation during heat shock response. *eLife* 3:e03164
111. Khanna N, Hu Y, Belmont AS. 2014. HSP70 transgene directed motion to nuclear speckles facilitates heat shock activation. *Curr. Biol.* 24:1138–44
112. Vitor AC, Sridhara SC, Sabino JC, Afonso AI, Grosso AR, et al. 2019. Single-molecule imaging of transcription at damaged chromatin. *Sci. Adv.* 5:eaau1249
113. Lionnet T, Singer RH. 2012. Transcription goes digital. *EMBO Rep.* 13:313–21
114. Nicolas D, Zoller B, Suter DM, Naef F. 2018. Modulation of transcriptional burst frequency by histone acetylation. *PNAS* 115:7153–58
115. Chen LF, Lin YT, Gallegos DA, Hazlett MF, Gomez-Schiavon M, et al. 2019. Enhancer histone acetylation modulates transcriptional bursting dynamics of neuronal activity-inducible genes. *Cell Rep.* 26:1174–88.e5
116. Senecal A, Munsky B, Proux F, Ly N, Braye FE, et al. 2014. Transcription factors modulate c-Fos transcriptional bursts. *Cell Rep.* 8:75–83
117. Hocine S, Vera M, Zenklusen D, Singer RH. 2015. Promoter-autonomous functioning in a controlled environment using single molecule FISH. *Sci. Rep.* 5:9934
118. Das S, Singer RH, Yoon YJ. 2019. The travels of mRNAs in neurons: Do they know where they are going? *Curr. Opin. Neurobiol.* 57:110–16
119. Eliscovich C, Singer RH. 2017. RNP transport in cell biology: the long and winding road. *Curr. Opin. Cell Biol.* 45:38–46
120. Martin RM, Rino J, Carvalho C, Kirchhausen T, Carmo-Fonseca M. 2013. Live-cell visualization of pre-mRNA splicing with single-molecule sensitivity. *Cell Rep.* 4:1144–55
121. Schmidt U, Basyuk E, Robert MC, Yoshida M, Villemin JP, et al. 2011. Real-time imaging of cotranscriptional splicing reveals a kinetic model that reduces noise: implications for alternative splicing regulation. *J. Cell Biol.* 193:819–29
122. Coulon A, Ferguson ML, de Turris V, Palangat M, Chow CC, Larson DR. 2014. Kinetic competition during the transcription cycle results in stochastic RNA processing. *eLife* 3:e03939
123. Vargas DY, Shah K, Batish M, Levandoski M, Sinha S, et al. 2011. Single-molecule imaging of transcriptionally coupled and uncoupled splicing. *Cell* 147:1054–65
124. Mor A, Suliman S, Ben-Yishay R, Yunger S, Brody Y, Shav-Tal Y. 2010. Dynamics of single mRNP nucleocytoplasmic transport and export through the nuclear pore in living cells. *Nat. Cell Biol.* 12:543–52
125. Ma J, Liu Z, Michelotti N, Pitchiaya S, Veerapaneni R, et al. 2013. High-resolution three-dimensional mapping of mRNA export through the nuclear pore. *Nat. Commun.* 4:2414
126. Siebrasse JP, Kaminski T, Kubitscheck U. 2012. Nuclear export of single native mRNA molecules observed by light sheet fluorescence microscopy. *PNAS* 109:9426–31
127. Ben-Yishay R, Mor A, Shraga A, Ashkenazy-Titelman A, Kinor N, et al. 2019. Imaging within single NPCs reveals NXF1's role in mRNA export on the cytoplasmic side of the pore. *J. Cell Biol.* 218:2962–81
128. Saroufim MA, Bensidoun P, Raymond P, Rahman S, Krause MR, et al. 2015. The nuclear basket mediates perinuclear mRNA scanning in budding yeast. *J. Cell Biol.* 211:1131–40
129. Sambandan S, Akbalik G, Kochen L, Rinne J, Kahlstatt J, et al. 2017. Activity-dependent spatially localized miRNA maturation in neuronal dendrites. *Science* 355:634–37

130. Haimovich G, Choder M, Singer RH, Trcek T. 2013. The fate of the messenger is pre-determined: a new model for regulation of gene expression. *Biochim. Biophys. Acta* 1829:643–53
131. Eliscovich C, Shenoy SM, Singer RH. 2017. Imaging mRNA and protein interactions within neurons. *PNAS* 114:E1875–84
132. Biswas J, Liu Y, Singer RH, Wu B. 2019. Fluorescence imaging methods to investigate translation in single cells. *Cold Spring Harb. Perspect. Biol.* 11:a032722
133. Buxbaum AR, Haimovich G, Singer RH. 2015. In the right place at the right time: visualizing and understanding mRNA localization. *Nat. Rev. Mol. Cell Biol.* 16:95–109
134. Liao YC, Fernandopulle MS, Wang G, Choi H, Hao L, et al. 2019. RNA granules hitchhike on lysosomes for long-distance transport, using annexin A11 as a molecular tether. *Cell* 179:147–64.e20
135. Bauer KE, Segura I, Gaspar I, Scheuss V, Illig C, et al. 2019. Live cell imaging reveals 3′-UTR dependent mRNA sorting to synapses. *Nat. Commun.* 10:3178
136. Katz ZB, English BP, Lionnet T, Yoon YJ, Monnier N, et al. 2016. Mapping translation 'hot-spots' in live cells by tracking single molecules of mRNA and ribosomes. *eLife* 5:e10415
137. Moissoglu K, Yasuda K, Wang T, Chrisafis G, Mili S. 2019. Translational regulation of protrusion-localized RNAs involves silencing and clustering after transport. *eLife* 8:e44752
138. Pizzinga M, Bates C, Lui J, Forte G, Morales-Polanco F, et al. 2019. Translation factor mRNA granules direct protein synthetic capacity to regions of polarized growth. *J. Cell Biol.* 218:1564–81
139. Tanenbaum ME, Gilbert LA, Qi LS, Weissman JS, Vale RD. 2014. A protein-tagging system for signal amplification in gene expression and fluorescence imaging. *Cell* 159:635–46
140. Morisaki T, Lyon K, DeLuca KF, DeLuca JG, English BP, et al. 2016. Real-time quantification of single RNA translation dynamics in living cells. *Science* 352:1425–29
141. Pichon X, Bastide A, Safieddine A, Chouaib R, Samacoits A, et al. 2016. Visualization of single endogenous polysomes reveals the dynamics of translation in live human cells. *J. Cell Biol.* 214:769–81
142. Wang C, Han B, Zhou R, Zhuang X. 2016. Real-time imaging of translation on single mRNA transcripts in live cells. *Cell* 165:990–1001
143. Yan X, Hoek TA, Vale RD, Tanenbaum ME. 2016. Dynamics of translation of single mRNA molecules in vivo. *Cell* 165:976–89
144. Boersma S, Khuperkar D, Verhagen BMP, Sonneveld S, Grimm JB, et al. 2019. Multi-color single-molecule imaging uncovers extensive heterogeneity in mRNA decoding. *Cell* 178:458–72.e19
145. Lyon K, Aguilera LU, Morisaki T, Munsky B, Stasevich TJ. 2019. Live-cell single RNA imaging reveals bursts of translational frameshifting. *Mol. Cell* 75:172–83.e9
146. Zhao N, Kamijo K, Fox PD, Oda H, Morisaki T, et al. 2019. A genetically encoded probe for imaging nascent and mature HA-tagged proteins in vivo. *Nat. Commun.* 10:2947
147. Pitchiaya S, Mourao MDA, Jalihal AP, Xiao L, Jiang X, et al. 2019. Dynamic recruitment of single RNAs to processing bodies depends on RNA functionality. *Mol. Cell* 74:521–33.e6
148. Heyer EE, Moore MJ. 2016. Redefining the translational status of 80S monosomes. *Cell* 164:757–69
149. Trcek T, Sato H, Singer RH, Maquat LE. 2013. Temporal and spatial characterization of nonsense-mediated mRNA decay. *Genes Dev.* 27:541–51
150. El-Brolosy MA, Kontarakis Z, Rossi A, Kuenne C, Gunther S, et al. 2019. Genetic compensation triggered by mutant mRNA degradation. *Nature* 568:193–97
151. Ma Z, Zhu P, Shi H, Guo L, Zhang Q, et al. 2019. PTC-bearing mRNA elicits a genetic compensation response via Upf3a and COMPASS components. *Nature* 568:259–63
152. Zheng Q, Ayala AX, Chung I, Weigel AV, Ranjan A, et al. 2019. Rational design of fluorogenic and spontaneously blinking labels for super-resolution imaging. *ACS Cent. Sci.* 5:1602–13
153. Jradi FM, Lavis LD. 2019. Chemistry of photosensitive fluorophores for single-molecule localization microscopy. *ACS Chem. Biol.* 14:1077–90
154. Greer CJ, Holy TE. 2019. Fast objective coupled planar illumination microscopy. *Nat. Commun.* 10:4483
155. Chatterjee K, Pratiwi FW, Wu FCM, Chen P, Chen BC. 2018. Recent progress in light sheet microscopy for biological applications. *Appl. Spectrosc.* 72:1137–69

156. Hansen AS, Woringer M, Grimm JB, Lavis LD, Tjian R, Darzacq X. 2018. Robust model-based analysis of single-particle tracking experiments with Spot-On. *eLife* 7:e33125
157. Chen M, Ma Z, Wu X, Mao S, Yang Y, et al. 2017. A molecular beacon-based approach for live-cell imaging of RNA transcripts with minimal target engineering at the single-molecule level. *Sci. Rep.* 7:1550
158. Baker MB, Bao G, Searles CD. 2013. The use of molecular beacons to detect and quantify microRNA. *Methods Mol Biol*. 1039:279–87
159. Ozawa T, Natori Y, Sato M, Umezawa Y. 2007. Imaging dynamics of endogenous mitochondrial RNA in single living cells. *Nat. Methods* 4:413–19
160. Zinskie JA, Roig M, Janetopoulos C, Myers KA, Bruist MF. 2018. Live-cell imaging of small nucleolar RNA tagged with the Broccoli aptamer in yeast. *FEMS Yeast Res*. 18:foy093
160a. Ye H, Rong Z, Lin Y. 2017. Live cell imaging of genomic loci using dCas9-SunTag system and a bright fluorescent protein. *Protein Cell* 8(11):853–55
161. Xue Y, Acar M. 2018. Live-cell imaging of chromatin condensation dynamics by CRISPR. *iScience* 4:216–35